scientific reports

Check for updates

OPEN

Unveiling a novel exopolysaccharide produced by *Pseudomonas alcaligenes* Med1 isolated from a Chilean hot spring as biotechnological additive

Shrabana Sarkar[1,9], Gustavo Cabrera-Barjas[2,9], Ram Nageena Singh[3,4], João Paulo Fabi[5,6], Sura Jasem Mohammed Breig[7], Jaime Tapia[8], Rajesh K. Sani[3,4] & Aparna Banerjee[1]✉

Exopolysaccharides (EPSs), a constitutive part of bacterial biofilm, act as a protecting sheath to the extremophilic bacteria and are of high industrial value. In this study, we elucidate a new EPS produced by thermotolerant (growth from 34–44 °C) strain *Pseudomonas alcaligenes* Med1 from Medano hot spring (39.1 °C surface temperature, pH 7.1) located in the Central Andean Mountains of Chile. Bacterial growth was screened for temperature tolerance (10–60 °C) to confirm the thermotolerance behaviour. Physicochemical properties of the EPS were characterized by different techniques: Scanning Electron Microscopy- Energy Dispersive X-ray Spectroscopy (SEM-EDS), Atomic Force Microscopy (AFM), High-Performance Liquid Chromatography (HPLC), Gel permeation chromatography (GPC), Fourier Transform Infrared Spectroscopy (FTIR), Nuclear Magnetic Resonance (NMR), and Thermogravimetric analysis (TGA). Whole genome of *P. alcaligenes* Med1 has also been studied in detail to correlate the structural and functional characteristics with genomic insight. The EPS demonstrated amorphous surface roughness composed of evenly distributed macromolecular lumps composed of mainly carbon and oxygen. The monosaccharide analysis has shown the presence of glucose, galactose, and mannose sugars at different ratios. TGA revealed the high thermal stability (315.3 °C) of the polysaccharide. The GPC has shown that Med1 is a low molecular weight polysaccharide (34.8 kDa) with low PI. The 2D-NMR linkage analysis suggests a diverse array of glycosidic bonds within the exopolysaccharide structure. The functional properties of the EPS were evaluated for food industry applications, specifically for antioxidant (DPPH, FRAP an H_2O_2). Extracted Med1 EPS revealed significant emulsification activity against different food grade vegetative oils (Coconut oil, Corn oil, Canola oil, Avocado oil, Sunflower oil, Olive oil, and Sesame oil). The highest 33.9% flocculation activity was observed with 60 mg L^{-1} EPS concentration. It showed water-holding (WHC) of 107.6% and oil-holding (OHC) capacity of 110.8%. The functional EPS produced by *Pseudomonas alcaligenes* Med1 from Central Andean Chilean hot spring of central Chile can be a useful additive for the food-processing industry.

Keywords *Pseudomonas*, Exopolysaccharide, Food industry, Additive, Biotechnology

[1]Functional Polysaccharides Research Group, Instituto de Ciencias Aplicadas, Facultad de Ingeniería, Universidad Autónoma de Chile, Sede Talca, Talca, Chile. [2]Facultad de Ciencias para el Cuidado de la Salud, Universidad San Sebastián, Campus Las Tres Pascualas, Lientur 1457, 4080871 Concepción, Chile. [3]Department of Chemical and Biological Engineering, South Dakota Mines, Rapid City, SD, USA. [4]2-Dimensional Materials for Biofilm Engineering, Science and Technology, South Dakota Mines, Rapid City, SD, USA. [5]Department of Food Science and Experimental Nutrition, School of Pharmaceutical Sciences, University of São Paulo, São Paulo, SP, Brazil. [6]Food Research Center (FoRC), CePID-FAPESP (Research, Innovation and Dissemination Centers, São Paulo Research Foundation), São Paulo, SP, Brazil. [7]Biology Department, Al-Rasheed University College, Baghdad, Iraq. [8]Instituto de Química de Recursos Naturales, Universidad de Talca, 3460000 Talca, Chile. [9]Shrabana Sarkar and Gustavo Cabrera-Barjas contributed equally to this work. ✉email: aparna.banerjee@uautonoma.cl

Hot spring is a polyextreme environment with several extreme environmental factors like high temperature, pH, metal concentration, and many more[1]. In such environment, to protect the cells from adverse environmental conditions, microbial cells produce extracellular carbohydrate polymers called exopolysaccharide (EPS)[2]. Even being a substantial component, EPS is influenced by altering the physical and biogeochemical microenvironment around the cells by giving them an option of reduced carbon reservoir as energy to survive. It is a complex high-molecular-weight architectural matrix comprising several inorganic compounds like polysaccharides, lipids, proteins, and nucleic acids, secreted due to the influence of the surrounding extreme habitat[3]. Due to structural chemistry, EPS showed a hydrophilic nature in an aqueous solution, having hydroxyl and carboxyl groups, which convey a net negative charge and provide acidic properties[4]. The EPS matrix may serve as a multipurpose functional element of microbial communities, including adhesion, structure, protection, recognition, and physiology[5]. It also has enough potential to be an important biotechnological component for further industrial use. However, due to its very complex structure, knowledge regarding EPS still needs to be completed. Much work is required to understand their precise roles in biotechnological applications fully.

Nowadays, the increased demand for natural polymers over synthetic ones focuses on natural sources for EPS with biotechnological applications[6]. Compared to plant polysaccharides, microbial EPS have a much greater variety of physicochemical properties and biological activities. Due to structural complexity, they act as emulsifiers to stabilize the emulsion effect between hydrophobic compounds and water. In addition, their nontoxic and biodegradable nature, environmental compatibility, and selectivity make bioactive compounds more favorable than artificial additives[7]. Several microbial EPSs, such as xanthan, gellan, and dextran, have already been widely applied in food industries[7]. In addition, EPS of thermophilic bacteria was found to have efficient functional characteristics, such as antioxidant, emulsification, and flocculation activity, which is useful for application in the food industry[8]. For example, EPS of thermophilic *Geobacillus* sp. showed complete emulsification against different edible food-grade oils[9]. On the other hand, EPS of a thermotolerant *Bacillus* has shown promising antioxidant activity similar to or higher than commercial ascorbic acid[10]. Due to its antiviral, antitumor, and immunoregulatory responses, EPS also get attention in biomedical, biomaterials, cosmetics, and wastewater treatment industries[11]. Therefore, studying extremophilic bacterial EPS will advance understanding and offer more opportunities for finding new EPS resources for biotechnological applications in the food industry as food additives.

Our present study reveals the biotechnological potential of a thermostable EPS produced by a thermotolerant bacteria isolated from an unexplored hot spring, Medano, located in the Maule region, Central Andean mountains of Chile, which is volcanic in origin, slightly acidic, and rich in metals. This sampling site is rich in probable bioactive compounds producing thermophilic bacterial communities. In the present study, a thermotolerant strain *Pseudomonas alcaligenes* Med1 was isolated and characterized for EPS production. The production has been optimized by statistical analysis followed by morphological and structural elucidation to understand the detailed chemical nature of the isolated EPS. The whole genome of *P. alcaligenes* Med1 has also been studied extensively, which provides clear genomic insight into EPS production. In addition, the EPS has also been explored in terms of biotechnological applications, such as emulsifiers and flocculating agents, water retention, and oil holding capacity. Due to showing the promising structural and functional propertied supported with genomic insights, the isolated EPS from thermotolerant *P. alcaligenes* Med1 can be used as a future food additive in industry.

Results

Sample collection from hot water spring

Medano is a hot spring (-35.5733, -70.7785) located in Maule of the Central Andean Mountain range of the central Chile region, which is an active volcanic zone. The water sample for the present study was collected from this hot spring. The surface water temperature of the study site was recorded to be 39.1 °C and the water of the hot spring was a little alkaline in nature (pH 7.10 ± 0.07). Other than that, serval physiochemical parameters: conductivity, DO, BOD, TDS, total alkalinity, chlorides, color, turbidity, nitrates, sulfates, Al, As, Cd, Cu, Cr, Fe, Mn, Mg, Hg, Ni, Pb, Se and Zn have also been studied. Detailed information on the physiochemical characteristics can be found in Table 1.

Isolation and taxonomic identification of EPS producing thermotolerant bacteria

Several individual colonies grew on nutrient agar plates at a temperature of 37 °C, of which one yellowish, shiny, mucoidal, convex, and opaque colony was isolated as Med1 for EPS production. Evaluation of temperature tolerance of the isolated bacteria revealed that it can tolerate the temperature upto 44 °C with an optimum growth temperature at 37 °C (growth range 34–44 °C) (See supplementary Fig. S1). According to pairwise nucleotide similarity values and phylogenetic inference methods in EZ-Taxon[12], 16 S rRNA sequence of Med1 (GenBank with accession number: MZ298608) showed 99.7% nucleotide identity with *P. alcaligenes* NBRC 14,159. Other than this, Med1 also demonstrated > 97% nucleotide identity with 27 different *Pseudomonas* strains. Therefore, Med1 had been identified as *Pseudomonas alcaligenes* Med1. The study site and the phylogenetic tree are presented in Fig. 1.

Whole genome sequencing, assembly, and annotation

Genomic DNA isolation and genome sequencing

The high quality gDNA was sequenced and obtained 412,416 super high-quality reads (1,952,584,919 bp) with N50 of 11.68 kb. The de-novo assembly of these reads resulted in a single circular chromosome genome consist of 4,091,487 bases, with of 467x coverage. The gene prediction obtained a total of 3915 genes including 3840 protein-coding genes (CDS), 65 tRNAs, 9 rRNA genes, and 1 tmRNA. The complete genome sequence (circular

Parameters	Units	Result
pH	-	7.10 ± 0.07
Conductivity	Ms cm^{-1}	1.88 ± 0.01
Total alkalinity	mg L^{-1} $CaCO_3$	32,3 ± 0,3
Aluminium (Al)	mg L^{-1}	< 0.02
Arsenic (As)	mg L^{-1}	0.20 ± 0.02
Cadmium (Cd)	mg L^{-1}	< 0.02
Cyanide (CN^-)	mg L^{-1}	< 0.005
Chloride (Cl^-)	g L^{-1}	0.70 ± 0.0
Copper (Cu)	mg L^{-1}	0.05 ± 0.00
Colour	Unit. Pt/Co	< 0.5
Chromium (Cr)	mg L^{-1}	0.003 ± 0.001
Biological oxygen demand	mg L^{-1}	< 0.2
Fluoride (F^-)	mg L^{-1}	1.2 ± 0.0
Iron (Fe)	mg L^{-1}	< 0.02
Manganese (Mn)	mg L^{-1}	< 0.02
Magnesium (Mg)	mg L^{-1}	2.67 ± 0.02
Mercury (Hg)	mg L^{-1}	< 0.0005
Níckel (Ni)	mg L^{-1}	0.030 ± 0.02
Nitrate (NO_3^-)	mg L^{-1}	< 0.05
Nitrite (NO_2^-)	mg L^{-1}	0.06 ± 0.00
Lead (Pb)	mg L^{-1}	< 0.02
Selenium (Se)	mg L^{-1}	< 0.0005
Sulfate (SO_4^{2-})	mg L^{-1}	116.8 ± 4.8
Total disolved solid	g L^{-1}	1.24 ± 0.01
Total suspended solid	mg L^{-1}	1.11 ± 0.5
Turbidity	NTU (Nephelometric Turbidity Unit)	< 0.2
Zinc (Zn)	mg L^{-1}	0.06 ± 0.01

Table 1. Analyses of water parameters of collected water sample from Medano hot spring.

chromosome) was deposited in GenBank as *Pseudomonas alcaligenes* Med1 under the accession number CP154874.

TYGS and ANI heatmap results indicate that strain Med1 has the highest similarity with the species *P. alcaligenes* NBRC 14,159 (Fig. 2A). JspeciesWS is a web-based server to identify genomes based on pairwise genome comparison. A Z-score value > 0.999 is considered as the above cutoff to identify the species accurately from the database of type strains. Also, according to the calculation done by the JspeciesWS, the isolated genome of Med1 has similarity with type strain *P. alcaligenes* NBRC14159 with a Z-score value of 0.99517, which again confirms the identity of the isolated bacterial strain and named *P. alcaligenes* Med1. Annotated circular genome had been mapped in Fig. 2B.

Determination of OrthoANI and heat map study

Overall genome relatedness is an important factor for species identification in prokaryote. According to recent research trends, the relatedness calculation based on genome sequence shows more accuracy in demarcating one species than DNA-DNA hybridization. Apart from this, analyzing the orthologous gene sharing also helps in understanding species-relatedness. Therefore, the identification of ortholog genes is important for predicting gene function in newly sequenced genomes[13]. In the present study, OAT was used for the determination of OrthoANI, followed by Heat Map formation. *P. alcaligenes* Med1 genome was compared with three more closely related strains and the type strain and revealed that all of the ANI values were higher than 85% (Fig. 2C). Genome relatedness confirms that Med1 is a member of the same clade. It shared 90.25% orthologous gene with *P. alcaligenes* NBRC14159 strain and more than 87% with the other two strains. Hence, Med1 is positioned in the same clade as *P. alcaligenes* NBRC14159, sharing the same orthologous genes.

Subsystem gene categorization, and identification of unique genes

The genome of *P. alcaligenes* Med1 consists of 4,091,487 bp with 66.6% GC content, out of which 3902 are coding sequences, and 67 RNAs are present (predicted from https://rast.nmpdr.org/seedviewer.). Uniqueness can be understood by identifying the common ancestral gene present in the genome. According to the annotation done by the RAST pipeline of *P. alcaligenes*, the Med1 genome contains 327 subsystems, 67 RNA coding genes, and 3902 coding sequences (CDS), along with 66.6% GC content. In addition, Annotation done by the RAST pipeline showed that 31% (1179) of the total protein-coding genes were within subsystems where, as 69% of the total coding genome (2723) was not covered by subsystems. The featured subsystem mainly included CDS

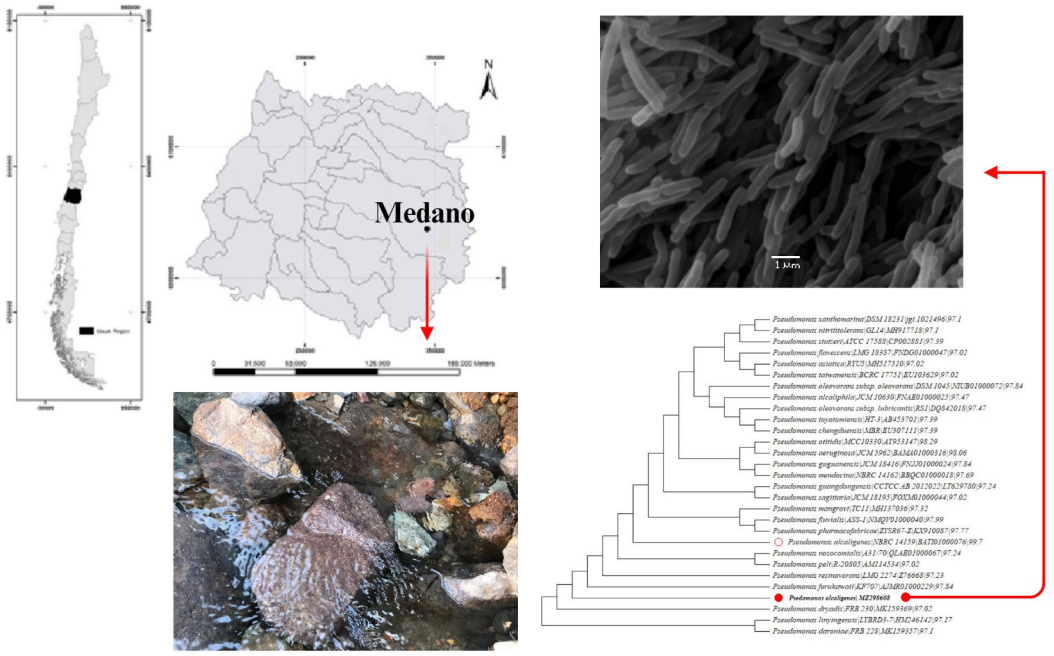

Fig. 1. Map showing the location of Medano hot spring located in the Andean Mountains in the Maule region, Chile, and photographs of the study site. On the right, the maximum likelihood phylogeny of isolate Med1 (marked with red arrow) shows similarity with *Pseudomonas alcaligenes*. On top right corner SEM micrograph demonstrating the morphology of the isolated Med1.

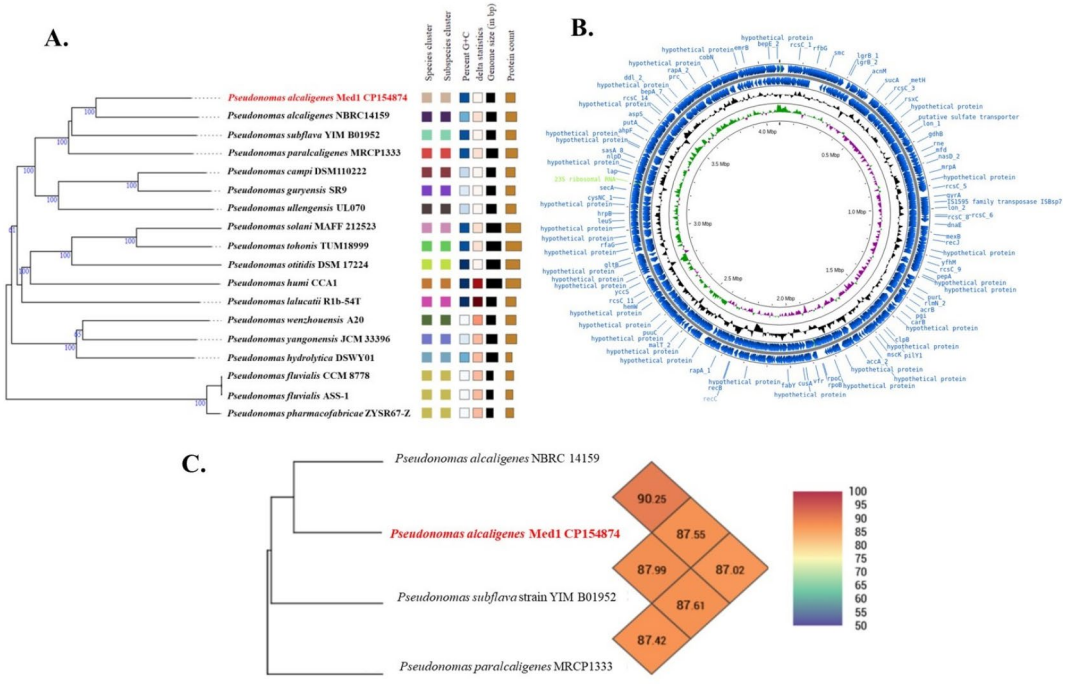

Fig. 2. (A) Phylogenetic tree showing maximum similarity within the species (B) Circular representation of annotated whole genome of *Pseudomonas alcaligenes* Med1 (C) Pairwise ANI% value-based heatmap showing maximum similarity within the species.

related to amino acids metabolism and derivatives (363) followed by protein metabolism (198) and carbohydrate metabolism (148). More specifically, extracellular polysaccharide-related genes like dTDP rhamnose, UDP N-acetylmuramate, etc., are present, indicating the synthesis of polysaccharides by the strain. dTDP-rhamnose (RfbA and RfbB) is often found to be covalently bound to the cell wall and exopolysaccharide, loosely associated with the cell wall of bacteria[14]. Interestingly, in the Med1 genome ABC-type polysaccharide/polyol phosphate export systems, permease component (9) is present to export synthesized polymer out of the cell to accumulate as exopolysaccharide. This belongs to the ATP-binding cassette (ABC) transporter superfamily responsible for the export of oligo- and polysaccharides in both Gram-positive and Gram-negative bacteria outside of the cell[15]. Specifically, the presence of genome related to rhamnose-containing polysaccharide translocation permease (rgpC) is a probable indicator of Med1 polysaccharide containing rhamnose. Apart from that capsular polysaccharide modification and export proteins are present. Putative glycosyltransferase was found, which is possibly involved in cell wall localization and side chain formation of rhamnose-glucose polysaccharide (rgpE) by catalyzing the glycosidic bond between sugar residues. Other proteins related to Polysaccharide export protein (Wza), polysaccharide ABC transporter, permease protein (RfbA-1), DNA for glycosyltransferase, Alpha-L-Rha alpha-1,2-L-rhamnosyltransferase/alpha-L-Rha alpha-1,3-L- rhamnosyltransferase (rgpF) are also identified in Med1 genome. The presence of *rgpE* gene indicates the possible synthesis of rhamnose-rich polysaccharides by Med1, as reported for the EPS production in the *Sinorhizobium fredii* HH103 [16].

In bacterial genome or plasmid can be analyzed for the presence of prophage sequence by PHASTEST, a web-based PHAge search tool[17]. It identified and annotated three regions for the presence of prophage. However, all three regions have a score of less than 90, indicating that the regions are either incomplete or questionable. The phage(s) with the highest number of proteins most similar to those in the region three most common phage has been predicted, PHAGE_Bacill_vB_BanS_Tsamsa_NC_023007, PHAGE_Pseudo_JBD25_NC_027992, PHAGE_Shigel_SfIV_NC_022749(2) (Fig. 3).

Foreign genetic material acquired by horizontal gene transfer can be predicted by analyzing the Genomic Island (GI)[18]. A total of 24 GIs were identified harboring genes responsible for cellular metabolism, EPS biosynthesis, metal resistance and other (Fig. 4). Among 23 identified GI, three GIs consisted of more than one GIs, GI-7, GI-16 and GI-23. GI-7 acquired GGDEF domain-containing protein responsible phosphorylation receiver or oxygen sensing domain ubiquitous in bacteria, DNA-binding transcriptional regulator protein family along with Mu-like prophage major head subunit gpT family protein, phage tail length tape measure family protein. GI-16 acquired different regulatory and stress response proteins like, SdiA-regulated domain-containing protein, TraR/DksA family transcriptional regulator, universal stress protein, inorganic anion transporter protein, phospholipase protein and other. GI-23 acquired virulence factor TspB C-terminal domain-related protein, outer membrane protein assembly factor BamC, phosphoribosyl aminoimidazole succino carboxamide synthase, regulator response proteins to stress. On the other hand, GI-3 acquired metal translocating P-type ATPase responsible to increase resistance against metals as stated before by Chien et al.,[19]. In case of *P. alcaligenes* Med1, genomic island results indicating metal translocating genes supports the metal-enriched geothermal environment from where the bacteria was isolated. Interestingly GI-5 contain exopolysaccharide biosynthesis polyprenyl glycosylphosphotransferase involve in synthesis of repeating unit important factor for EPS biosynthesis as stated before by Audy et al.,[20]. GI- 20 contains glycosyltransferase family 1 protein which support the exopolysaccharide production by bacteria. This is a polyphyletic multigene family, comparisons of UDP-glycosyltransferases (UGTs) from plants, animals, fungi, bacteria, and viruses reveal the presence in distinct

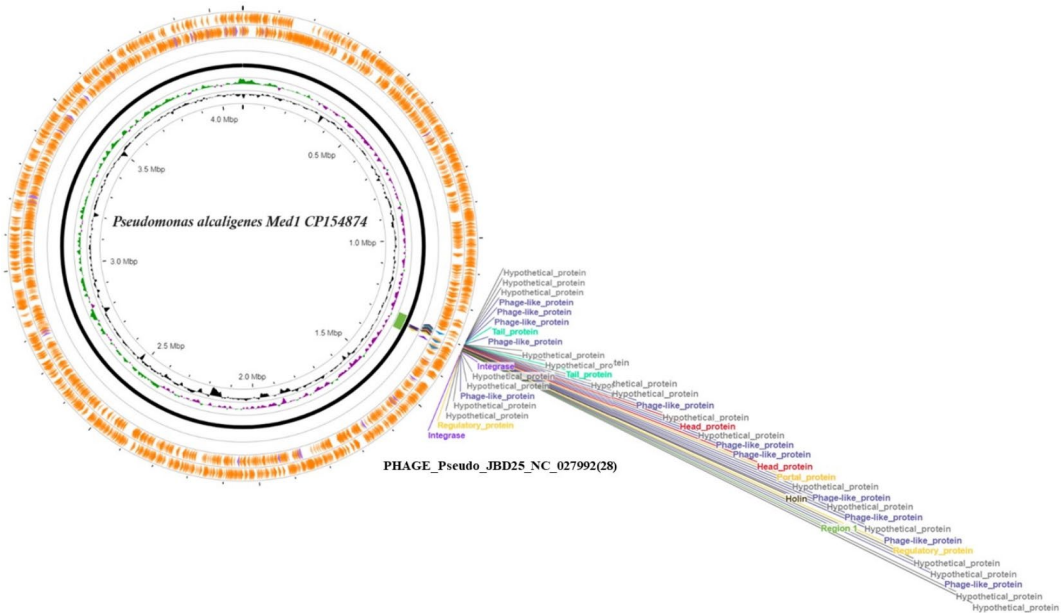

Fig. 3. Circular genomic map of Med1 obtained from PHASTEST.

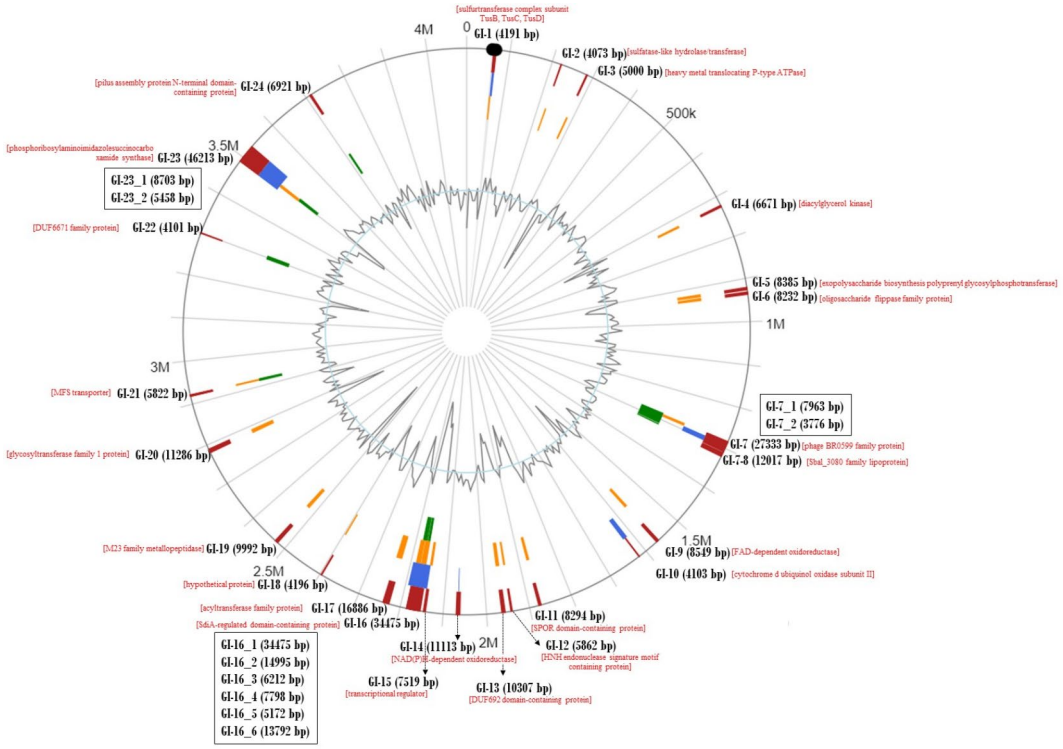

Fig. 4. Demonstrating Genomic Islands predicted from the genome of *Pseudomonas alcaligenes* Med1.

clades. Minor clade contains lipid glycosyltransferase clade homologous to bacterial lipid glycosyltransferases reflects the bacterial origin of chloroplasts proves the horizon gene transfer between different clades[21].

Biosynthetic gene cluster analysis

The Biosynthetic gene cluster (BGC) analysis resulted in 9 BGC clusters 1.1 to 1.9 (Fig. 5A to 5I). The BGCs include biosynthetic genes in two categories Core biosynthetic genes (CBGs) and additional biosynthetic genes (ABG). Where BGC 1.1 (Fig. 5A) has 34 genes (PSAMED_00270-PSAMED_00304) includes 2 genes (PSAMED_00290–291) as CBGs for the biosynthesis of Linear gramicidin synthase subunit B and a single gene for L-ornithine N(5)-monooxygenase (PSAMED_00287). There were 4 more genes categorized as ABGs such as PSAMED_00288, 00292, 00293, and 00296 codes for N(6)-hydroxylysine O-acetyltransferase, Linear gramicidin dehydrogenase LgrE, Protein MbtH, and Phthiocerol synthesis polyketide synthase type I PpsC respectively. The second BGC (Fig. 5B) has 17 genes (PSAMED_00311-PSAMED_00327) including 2 genes as CBGs such as 3-hydroxy-3-isohexenylglutaryl-CoA/hydroxy-methylglutaryl-CoA lyase (PSAMED_00319) and Acetyl-coenzyme A synthetase (PSAMED_00320) and 5 genes as ABGs such as PSAMED_00312, PSAMED_00315–00318 encodes for (R)-benzylsuccinyl-CoA dehydrogenase, Acyl-CoA dehydrogenase, Methylmalonyl-CoA carboxyltransferase 12 S subunit, 2,3-dehydroadipyl-CoA hydratase, and Acetyl-/propionyl-coenzyme A carboxylase alpha chain respectively. The third BGC (Fig. 5C) has 13 genes (PSAMED_00851–00863), which include 3 genes (PSAMED_00857–00859) as CBGs for the biosynthesis of Asparagine synthetase [glutamine-hydrolyzing] 1, Glutathione biosynthesis bifunctional protein GshAB, and hypothetical protein respectively. However, it has 2 genes in ABG category PSAMED_00851 and PSAMED_00855 that encodes for tRNA 5-methylaminomethyl-2-thiouridine biosynthesis bifunctional protein MnmC and Beta-lactamase hydrolase-like protein respectively. The fourth BGC (Fig. 5D) has 49 genes (PSAMED_01653–01701). It has 2 genes PSAMED_01680 (encodes hypothetical protein) and PSAMED_01684 (encodes 3-oxoacyl-[acyl-carrier-protein] synthase 3) as CBG and 11 genes (PSAMED_01653, 01654, 01654, 01660, 01673, 01679, 01694, 01695, 01696, 01700, and 01701). These genes encode Poly(3-hydroxyalkanoate) polymerase subunit PhaC, 3-oxoadipate enol-lactonase 2, Poly(3-hydroxyalkanoate) polymerase subunit PhaC, Ubiquinone/menaquinone biosynthesis C-methyltransferase UbiE, Proline iminopeptidase, hypothetical protein, 3-methylmercaptopropionyl-CoA dehydrogenase, hypothetical protein, 3-methylmercaptopropionyl-CoA dehydrogenase, Malonyl-[acyl-carrier protein] O-methyltransferase, and Pimeloyl-[acyl-carrier protein] methyl ester esterase respectively. The fifth BGC (Fig. 5E) was identified as RiPP-like region and has 10 genes (PSAMED_01883–01892) which include only gene (PSAMED_01888) as CBG encodes for hypothetical protein. The sixth BGC (Fig. 5F) has 40 genes (PSAMED_02732–02771). It has 2 genes (PSAMED_02747 and 02750) in the CBG category and encodes 3-oxoacyl-[acyl-carrier-protein] synthase 2. The sixth BGC identified as T1PKS, hglE-KS, has 10 genes as ABGs (PSAMED_02739, 02742, 02748, 02752, 02753, 02760, 02761, 02763, 02764, 02765 encode for 3-dehydroquinate synthase, Glutamate synthase [NADPH] small chain, 3-oxoacyl-[acyl-carrier-protein] reductase FabG, Trans-aconitate 2-methyltransferase, hypothetical protein, hypothetical

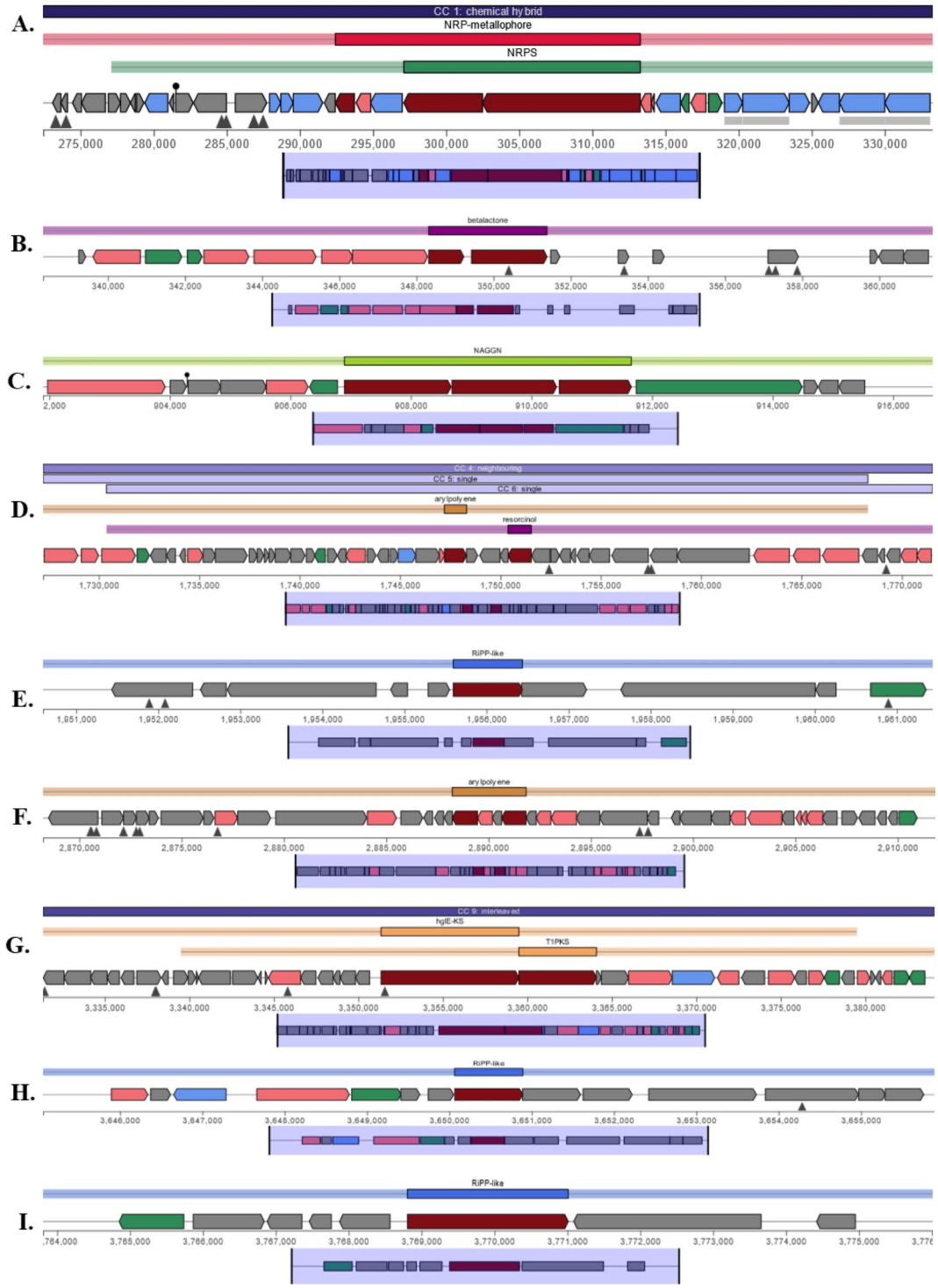

Fig. 5. Biosynthetic Gene Cluster Analysis of *Pseudomonas alcaligenes* Med1.

protein, Acetyl-coenzyme A synthetase, Acyl carrier protein, Acyl carrier protein, and hypothetical protein Respectively. The seventh BGC (Fig. 5G) has 39 genes (PSAMED_03167–03205). It has only 2 genes as CBGs (PSAMED_03187 and 03188) and both encode hypothetical proteins. It has 7 genes (PSAMED_03181, 03191, 03193, 03195, 03197, 03200 and 03203) as ABGs and encodes for Bifunctional enzyme CysN/CysC, Putative aminoacrylate hydrolase RutD, Putidaredoxin reductase CamA, hypothetical protein, hypothetical protein, putative oxidoreductase, and hypothetical protein respectively. The eight BGC (Fig. 5H) was identified as RiPP-like and has 14 genes (PSAMED_03476–03489). This BGC has one gene (PSAMED_03483) as CBG that encodes a hypothetical protein and 2 genes (PSAMED_03476 and 03479) as ABGs encode for hypothetical protein and Beta-ketodecanoyl-[acyl-carrier-protein] synthase respectively. The ninth BGC was also identified as RiPP-like

(Fig. 5I) and has 8 genes (PSAMED_03613–03620). This cluster has only one CBG (PSAMED_03618) that encode hypothetical protein.

Pan, core and accessory genome characteristics determination

The whole genome of Med1 gave a probable intimation of the presence of unique accessory genome. Accessory regions were found to be rich in genes related to membrane transport, cell wall and capsule, carbohydrate, however core genome is rich in stress response related genes compared to accessory genome. Sharing of genes and interrelationship among pan, core and accessory is depicted in Fig. 6A. According to present study, GC content of the accessory region (66.04%) was little lower than that of core genome (67.29%) in Med1. More specifically, accessory genome for Med1 constituted of nearly 18.8% of the total genome. However, percentage of accessory genome region was found 27.69% for *P. alcaligenes*, 34.14% for *P. paralcaligenes* and 23.07% for *P. subflava*. The average size of the accessory genome was 7142 kbp. of total genome in entire reference set, which indicate the size of identified unique gene comparatively higher. The pangenome and accessory genome shows a total of 103 shared genes (Fig. 6B). Similar kind of study was done before where 11,760 accessory genomes had been found in reference set of 8 *P. pseudoalcaligenes* strains[22]. In the present ClustAGE analysis, the final obtained subelement was found to be distributed into a total of 300 bins. Clustering similar accessory genome elements (AGEs) pooled together into bins was done in ClustAGE analysis by doing single nucleotide BLAST analysis[23]. A set of nucleotides of accessory genome elements (AGEs) was determined from AGEnt to cluster them for recognizing the minimum set of accessory genomic elements in the population[24]. This also helps to understand the distribution of each accessory genomic element among the genomes. The outermost ring represents the distribution of the bin according to different categories of genetic elements.

Optimization of media components for EPS production using response surface methodology (RSM)

Recovery, purification and EPS production optimization using Central Composite Design (CCD)

The CCD-based response surface methodology (RSM) technique was used to standardize the media composition with carbon and nitrogen source, pH of the media and bacterial concentration for EPS production by Med1 as done before by Kanmani et al.,[25] and Preetha et al.,[26]. There were 13 runs for each study consisting of the lowest to the highest value of all four factors (Fig. 7). Analysis of variance (ANOVA) for EPS production was shown in Table 2; the quadratic correlation model shows a significant P- value > F was < 0.0001 (Fig. 8). Additionally, the model was evaluated by determination of correlation coefficient R^2 = % 99.33 mean %0.67 of total experiments are not explained by the model, R^2 adjust, R^2 predict for EPS production were 0.98 and 0.96 respectively. Measurement of signal to noise model assessed by adequate precision accepted with value more than 4 in this model 49.63. From ANOVA Table 2 for EPS production, it can be noticed all terms exhibited significant effect ($P < 0.0001$) except AC, AD, BD, CD, A^2, C^2, and D^2 terms. C-pH was the most effective parameter from the highest F-value (184.52) on EPS production. In this study, the significance parameters were evaluated by F-value because all p-values showed < 0.0001, as also found before by Breig et al.,[27]. Furthermore, a regression optimization model was constructed which is a relationship between independent parameters and dependent parameters (EPS production) developed after ANOVA and regression coefficient determined, the CCD design matrix was fitted with a quadratic optimization model for EPS production in codded parameters as described in Eq. 1 as said before by Mohammed and Luti[28].

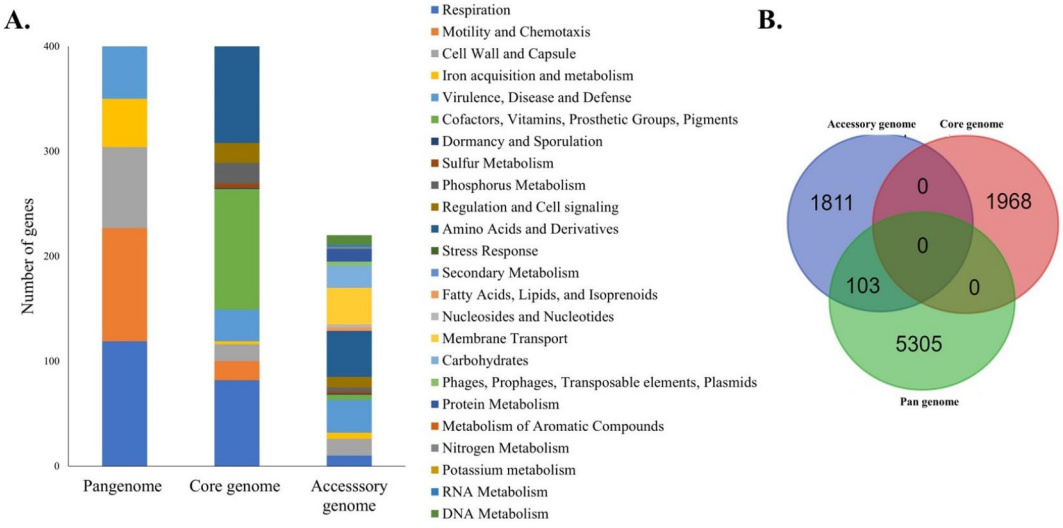

Fig. 6. Relative distribution of pan, core and accessory genome through Spine and Agent tool plotting each category or subcategory.

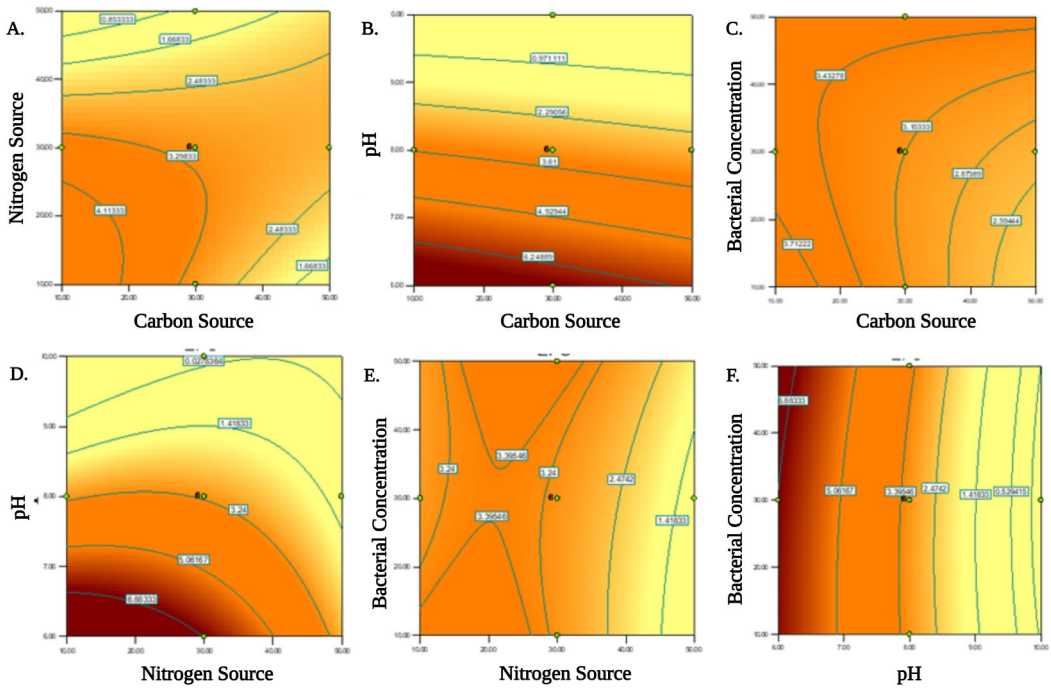

Fig. 7. Response surface plot (2-D) interaction effect expressed, respectively, in X1 and X2 axes. Here, inputs are 30 experimental runs carried out under conditions established by CCD matrix. EPS production as function with (A) nitrogen source (g L^{-1}) and carbon source (g L^{-1}) (B) carbon source (g L^{-1}) and pH (C) bacterial concentration and carbon source (mL L^{-1}) (D) nitrogen source (g L^{-1}) and pH (E) nitrogen source (g L^{-1}) and bacterial concentration (mL L^{-1}) and (F) pH and bacterial concentration (mL L^{-1}).

$$\begin{aligned} \mathrm{EPS} = {} & +3.15 - -0.22 * \mathrm{A} - 0.51 * \mathrm{B} - 1.76 * \mathrm{C} + 0.097 * \mathrm{D} + 0.36 * \mathrm{A} * \mathrm{B} + 0.072 * \mathrm{A} * \mathrm{C} + 0.10 * \mathrm{A} * \mathrm{D} \\ & + 0.48 * \mathrm{B} * \mathrm{C} + 0.11 * \mathrm{B} * \mathrm{D} - 0.042 * \mathrm{C} * \mathrm{D} - 7.292\mathrm{E} - 004 * \mathrm{A}^2 - 0.27 * \mathrm{B}^2 + 0.043 * \mathrm{C}^2 + 0.049 * \mathrm{D}^2 \end{aligned} \quad (1)$$

Contour plots (2-D) were graphical representations that helped the researcher visualize the current state of the regression optimization model and deduce the relationship between parameters and response. In this study, the relation between independent factors and response EPS production was visualized by 2D contour plots of the response surface. At the same time, others hold at zero level (coded value) was also found before by Breig et al.,[27] and Mohammed and Luti[28]. In Fig. 7, maximal production of EPS (4.11 g L^{-1}) was obtained when carbon source and nitrogen source concentrations were 19 g L^{-1} and 25 g L^{-1}, respectively, while minimum point with high concentrations of carbon source and nitrogen source. Figure 3 explains the linear change of EPS production from 6.2 g L^{-1} at acidic pH to 0.97 g L^{-1} at alkaline pH. Figure 7 showed a maximum EPS production of 3.71 g L^{-1} at a carbon source concentration of 17 g L^{-1} and 21 ml L^{-1} bacterial concentration of. The interaction between nitrogen source concentration and pH was explained in Fig. 7, where maximum production of EPS was obtained with a low range of nitrogen source concentration (10–30 g L^{-1}) and acidic to neutral pH. In Fig. 7D, linear change of EPS production also appears with pH and nitrogen source interactions, where maximum production of EPS (5.06 g L^{-1}) exhibited with acidic pH and minimum production (0.52 g L^{-1}) with alkaline pH. Figure 7E explains the interaction between nitrogen source (20 g L^{-1}) and bacterial concentration (25 g L^{-1}), showing maximum production of EPS of 3.39 g L^{-1}.

Validation of optimum condition To validate the obtained optimization result and model accuracy an experiment was carried out in the laboratory with the optimum condition suggested carbon source 30 g L^{-1}, nitrogen source 30 g L^{-1}, pH 7 and bacterial concentration 20 ml L^{-1} as shown in Fig. 8. Based on the optimization model, a ramp chart for optimization condition was developed by Design expert software (version 7) as shown in Fig. 8C. In triplicate the result revealed actual EPS yield 6.8 g L^{-1} which is good aggregate with predicted result.

Physicochemical characterization of the EPS

Morphological analysis (SEM-EDS and AFM)

A highly compact, amorphous, non-porous nature with flake-like surface morphology was observed for Med1 EPS at high magnification (3000× and 5000× magnification) in Field emission scanning electron micrograph (Fig. 9A-C). Chen et al.,[29] and Yadav et al.,[30] observed this kind of structural configuration for EPS previously in their studies also. However, the morphology of the biopolymer may differ according to the isolation and extraction procedure along with the physicochemical properties[31]. High-resolution topographical imaging revealed EPS's structure and distribution pattern[32]. The key non-metal elements present in EPS can be revealed

Source	Sum of squares	df	Mean square	F value	*p*-value Prob > F	
Model	90.8741	14	6.491005119	160.6264757	< 0.0001	Significant
A- Carbon source	1.1137	1	1.113704167	27.55973412	< 0.0001	
B- Nitrogen source	6.15094	1	6.1509375	152.2111591	< 0.0001	
C- pH	74.6595	1	74.6595375	1847.52564	< 0.0001	
D- Bacterial concentration	0.2262	1	0.226204167	5.597650504	0.0319	
AB	2.05206	1	2.05205625	50.78020388	< 0.0001	
AC	0.08266	1	0.08265625	2.045412365	0.1732	
AD	0.16606	1	0.16605625	4.109229574	0.0608	
BC	3.75391	1	3.75390625	92.8942005	< 0.0001	
BD	0.20026	1	0.20025625	4.955543106	0.0418	
CD	0.02806	1	0.02805625	0.694280235	0.4178	
A^2	1.5E-05	1	1.45833E-05	0.000360879	0.9851	
B^2	2.06644	1	2.066436012	51.13604561	< 0.0001	
C^2	0.05076	1	0.050764583	1.256220872	0.2800	
D^2	0.06659	1	0.066586012	1.647738097	0.2187	
Residual	0.60616	15	0.040410556			
Lack of fit	0.54703	10	0.0547025	4.625352311	0.0524	Not significant
Pure error	0.05913	5	0.011826667			
Cor total	91.4802	29				
Standard Deviation	0.20					
Mean	3.007					
Coefficient of variation (%)	6.68					
PRESS	3.23					
R^2	0.9933					
Adjusted R^2	0.987					
Predicted R^2	0.964					
Adequate precision	49.63					

Table 2. ANOVA analysis for EPS production from *Pseudomonas alcaligenes* Med1. Where df = degree of freedom, Cor Total = Corrected Total Sum of Squares, PRESS = prediction error sum of squares.

from EDS spectrum. The EDS spectrum of Med1 EPS confirmed the dominance of elements with carbon (58.94% of total weight) followed by oxygen (41.06% of total weight). Absence of N, P and S indicates a low chance of having protein and other undesired contaminants in the extracted EPS (Fig. 9C).

In the atomic force micrograph, a three-dimensional (3D) topographical image of Med1 EPS showed amorphous surface roughness with irregular lumps with spike-like heights ranging ~ 11 nm (Fig. 9D). The surface topographical two-dimensional (2D) image confirmed that these macromolecules are actually impregnated scattered particles with spherical surface topography.

Monosaccharide composition analysis

HPLC chromatogram was analyzed to understand the sugar composition of EPS produced by *P. alcaligenes* Med1 (Fig. 10A). It is a heteropolymer in nature, chemically composed of glucose: 21.78 mg g^{-1} (0.121 mol), galactose: 14.53 mg g^{-1} (0.081 mol), and mannose: 62.25 mg g^{-1} (0.346 mol). No other monosaccharides were detected using this method.

Determination of molecular weight

The Med1 heteropolysaccharide molecular weight and polydispersity index (PI) were the following: Mw 34.8 kDa, Mn 23.9 kDa and (polydispersity index) PI 1.46. These results indicates that it is a low molecular weight polysaccharide with a low polydispersity.

Thermogravimetric analysis

The thermogravimetric curve demonstrates a dynamic relation between weight loss and temperature to understand the thermal stability of EPS from *P. alcaligenes* Med1. In addition, being an important factor for industrial use, the determination of the thermal stability of EPS was performed for further biotechnological application on EPS in the food industry. Thermal decomposition curves (TG and DTG) of EPS *P. alcaligenes* Med1 are presented in Fig. 10B. Two distinct degradation peaks had been observed in the TGA curve. The first thermal degradation effect at a temperature range of 20–180 °C with maximum degradation rates at a temperature (T_{peak}) of 83.0 °C accounts for only 12.5% mass loss. This effect belongs to unbound water loss. In the temperature interval from 200 to 500 °C a second and most significant weight loss happened. The maximum decomposition rate occurred at a temperature (T_{peak}) of 315.3 °C with an associated mass weight loss of 53.3%.

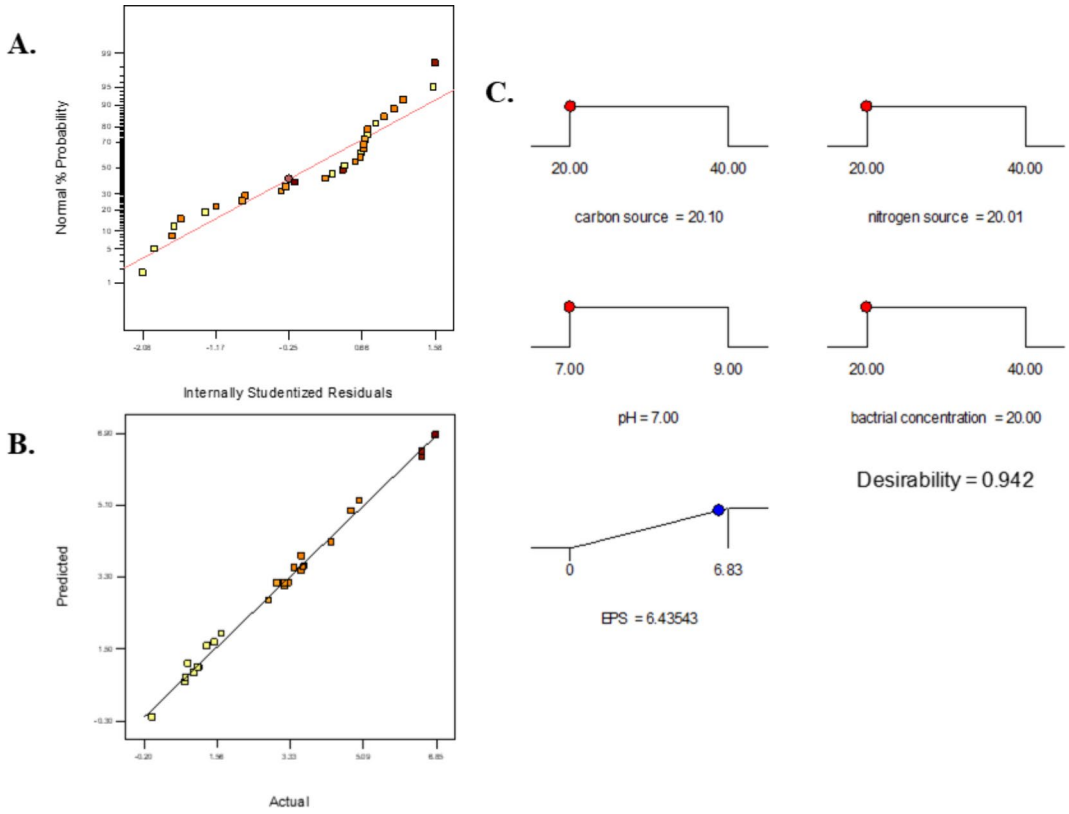

Fig. 8. (A) Normal plot of residuals; (B) Predicted versus actual plot for EPS production and (C) Ramp chart for optimization conditions of EPS production by Med1, developed by Design Expert software.

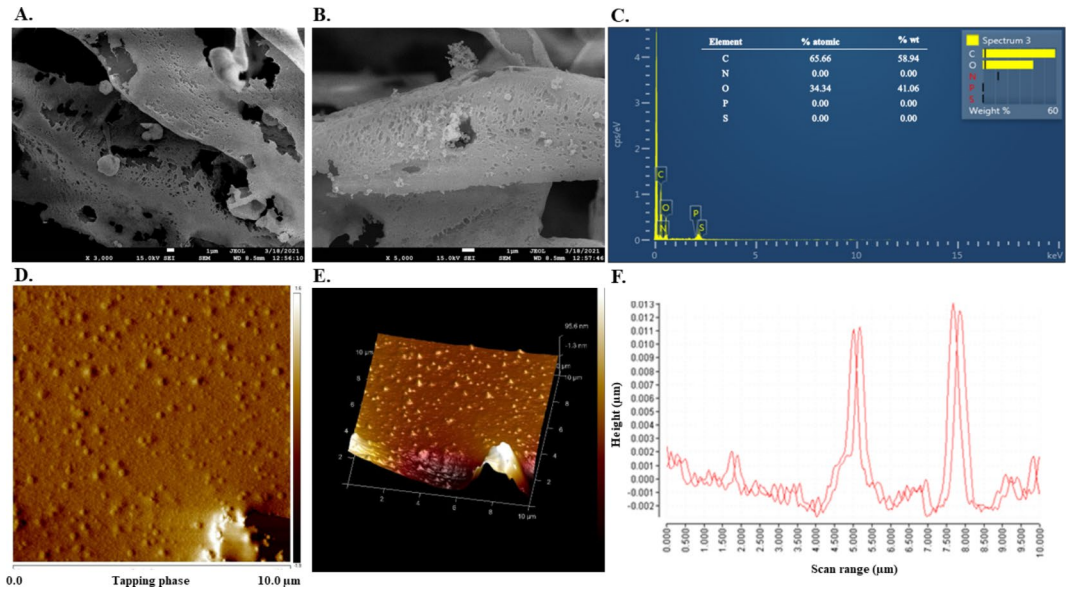

Fig. 9. Surface morphology of the EPS produced by *Pseudomonas alcaligenes* Med1, where (A) ×3000 (B) ×5000 respectively; and (C) energy dispersive X-ray spectroscopy (EDS) (D) 2D; and (E) 3D AFM images, and (F) size distribution patterns.

During this stage, a simultaneous decomposition processes could be occurring (chain hydrolysis, ring opening and rearrangement, water, carbon dioxide and volatile compounds releasing) as stated before by Wang et al.,[7]. This is followed by a residual decomposition of the polysaccharide, which is indicated by the broad extension of the process.

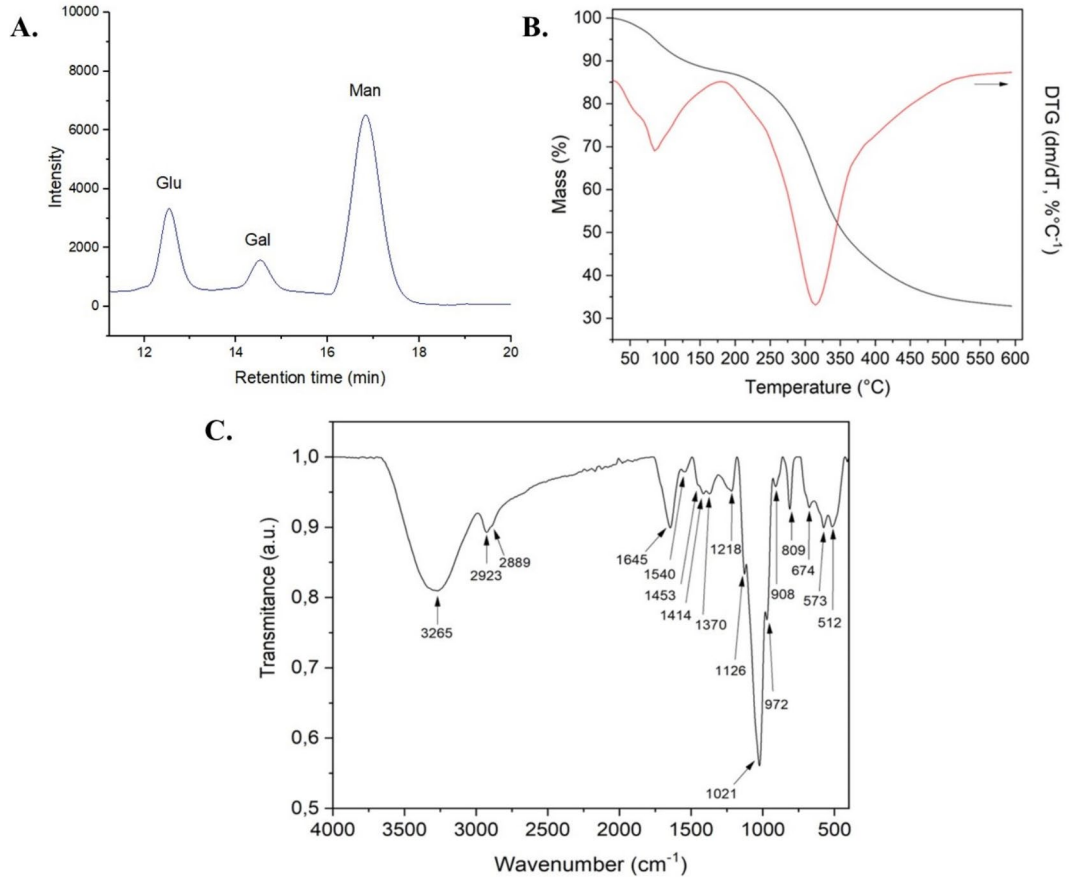

Fig. 10. (A) HPLC analysis of the constituting monosaccharides of the Med1 EPS. (B) Thermogravimetric curves of Med1 exopolysaccharide (C) FTIR-ATR spectra of Med1 polysaccharide.

Fourier transform infrared (FTIR) Spectroscopy analysis

P. alcaligenes Med1 derived EPS powder was analyzed by IR spectrum to detect the functional groups by their absorption band spectrum assignment (Fig. 10C). The absorption band in a region of 2923 cm^{-1} indicates the presence of (ν-C-H) stretching vibration, as Sabando et al.,[33] also found. Peaks at a region of 1540 cm^{-1} indicate stretching vibration for (ν-C-N (C-N-H) + δNH, Amide II). The presence of this functional group indicates protein traces in the EPS, as stated before by Wang et al.,[34]. The presence of (δ-CH + δC-CH3) due to C-H groups can be confirmed from the vibrated stretch at a region of 1370 cm^{-1}, as Banerjee et al.,[8] mentioned. Peaks appear at a range of 1000–1200 cm^{-1} (like 1021 cm^{-1}, 1126 cm^{-1},) indicating the presence of β– (1–4) linkage; however, adjacent peaks (like 1218 cm^{-1}) appear due to the (1–3) linked β-glucan[35]. Absorption peaks at 972 cm^{-1}, 908 cm^{-1}, 809 cm^{-1}, and 674 cm^{-1} were also observed. Stretching vibration at a region of 1200 –950 cm^{-1} hints at a sugar region with an intense overlapping, as stated by Synytsya et al.,[36]. The clear band at 809 cm^{-1} indicates the presence of mannose in the α-anomeric configuration (γCH C1 axial of α- linkage) as a monomeric sugar unit of EPS[37].

Nuclear magnetic resonance (NMR) spectroscopy analysis

Analyzing the ^{1}H NMR (Fig. 11A), some peaks in the region between 4.25 and 3.5 ppm can be observed, which are related to the proton resonance of H2-H6 from several monosaccharides. It is also possible to observe a higher incidence of peaks from 5.1 to 5.8 ppm, characteristic of α-configuration of monosaccharides' anomeric proton. Analysis of ^{1}H NMR spectral data revealed distinctive chemical shifts indicative of D-mannopyranosyl residues. The prominent signal at 4.699 ppm was attributed to the non-reducing end of D-mannopyranosyl units (R). Signals corresponding to α-D-mannopyranosyl linkages (A, B, C, D) and less intense peaks associated with β-D-mannopyranosyl (E, F) were noted. In a deviation from previous observations, the typical chemical shifts for β-D-mannopyranosyl in the range of 4.5–4.7 ppm were absent, suggesting the presence of a diverse array of glycosidic bonds within the exopolysaccharide structure[38], demonstrating the EPS has a mixture of different glycosidic linkages. The signal from the anomeric proton at a chemical shift of 5.365 ppm aligns with phosphorylated mannose residues since phosphorus was roughly detected in the SEM-EDS analysis. This could be due to the superior sensitivity of NMR in detecting such spectra, even though it was observed with minimal intensity[39].

A more rigorous analysis using HSQC (Heteronuclear Single Quantum Correlation) 2D-NMR was done to depict the glycoside linkages and a possible chemical structure of the exopolysaccharide. Due to the complex

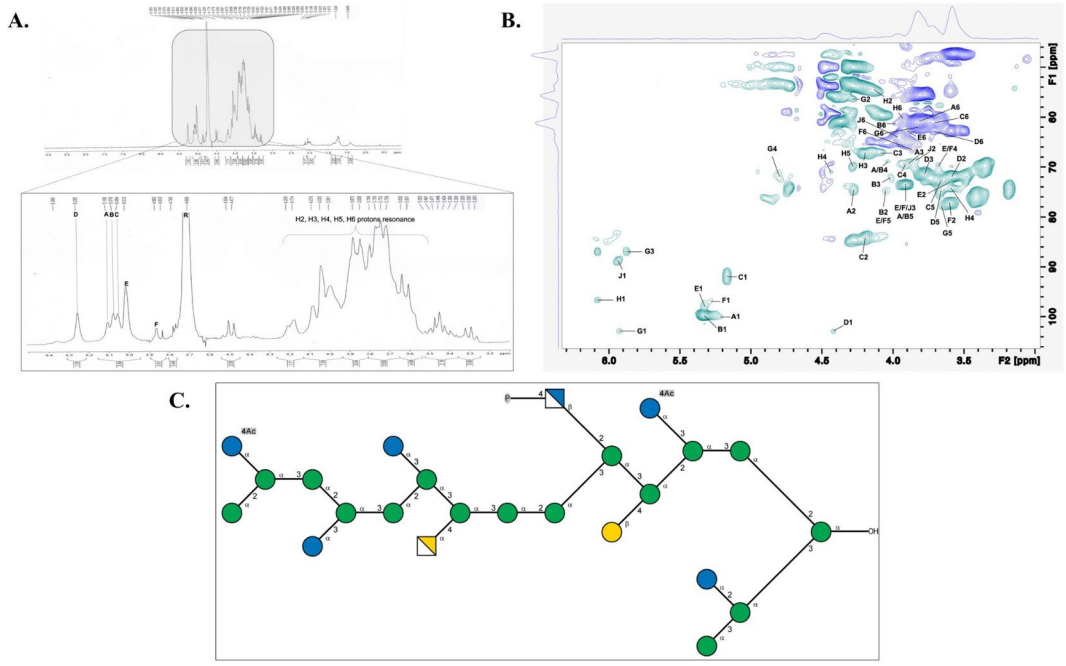

Fig. 11. (A)^{1}H NMR spectra, (B) HSQC ^{13}C/^{1}H NMR spectrum, and (C) probable structure of a new galactoglucomannan as the main exopolysaccharide produced by thermotolerant *Pseudomonas alcaligenes* Med1. The structure was created following the symbol nomenclature[44] for glycans guidelines and respecting the percentage quantity of each monosaccharide found after integrating the anomeric carbon regions.

structure, several tools were applied to identify the chemical shifts between ^{1}H and ^{13}C NMR. First, the Carbohydrate Structure Database (CSDB) was used to seek specific chemical shifts[40,41] identified in the TopSpin 4.3.1 software. Each ^{1}H/^{13}C pair of the chemical shift was used as an input of the CSDB, and together with a literature search for specific exopolysaccharides containing mannose, glucose, and galactose, the indicated glycosidic linkages were assumed. Afterward, the specific ^{1}H/^{13}C chemical shifts were again analyzed in CSDB[42,43] confirming the glycoside linkages and assuming a probable main structure of the studied exopolysaccharide using The Symbol Nomenclature for Glycans (SNFG)[44,45].

First, the anomeric region was screened for the anomeric carbons and hydrogens. Six primary spectra (A1-F1) were found. When integrated the areas, the higher values were achieved for the proposed backbone of the exopolysaccharide, mainly formed by [→1)-α-Manp-(2→] (A1) and [→1)-α-Manp-(3→] (B1), with a predominant spectrum of terminal α-Manp- (C1), also demonstrating a medium-to-low molecular weight polysaccharide (Fig. 11B). Similar kind of low molecular weight polysaccharide like Med1 EPS had also been reported before from *Pseudomonas* PT-8 EPS (7.3 kDa)[46]. Both glycoside linkages were found in the lipopolysaccharide structures of different bacteria[47–49]. It was seen as the second predominant linkage between the [→1)-α-Glcp-(3→] (E1) and [→1)-α-Glcp-(2→] (F1), with no terminal α-Glcp spectrum found. Conversely, the literature found for those types of glycosidic bonds was from exopolysaccharides produced by some probiotics[50,51]. At least, only a beta-linkage was found as being [→4)-β-Galp-(1→] (D1), with the smallest integrated area. Moreover, this linkage type, mainly in alpha-mannans found in lipopolysaccharides, is a ramified feature of diverse galactomannans[52–54]. When comparing the total integrated regions in the anomeric spectrum (A1-F1), a proportion of 10:3:0.3 (Man: Glc: Gal) was found, very similar to what had been achieved by the monosaccharide composition. Three more anomeric carbons were found as G1, H1 and J1 being →1)-β-GlcpN-(2→, →1)-α-GalpN-(4→, and →1)-α-Glcp-(3→, respectively, with G1 and J1 showing a C4 residue (acetate and phosphate groups, respectively). The observed sugars were also found in lipopolysaccharides from different bacteria[55–57] and the acetate groups were found in polysaccharides modified by *Lactobacillus bulgaricus* L3 β-galactosidase[58]. Following the analysis with other spectra, it was possible to assign most of the different hydrogen and carbon spectra (A2-J2 to A6-J6). Some spectra were duplicated, so they were indicated in the figure as both assignments. All assignments followed the above-explained methodology, with all features corresponding to the anomeric hydrogen and carbon seeking for literature and correspondently cited before. HMBC (Heteronuclear Multiple Bond Correlation) analysis confirmed the main backbone of the polysaccharide is formed by →1)-α-Manp-(2→ and→1)-α-Manp-(3→ (See supplementary Fig. S2, and Table S1). Only D4 and J5 could not be assigned since they represent the lowest sugar proportion (galactose) because those linkage features were completed and maintained the sugar proportion. The continued analysis integrating the anomeric carbon shifts depicted an exopolysaccharide structure considering the percentage quantity of each monosaccharide found (Fig. 11C), demonstrating a new galactoglucomannan was isolated[44]. Several other experiments should be done to ascertain the complete structure, such as repeating units and branching. Still, this approach was enough to predict a new exopolysaccharide produced by thermotolerant *P. alcaligenes* Med1.

Functional properties elucidation

In vitro antioxidant activity determination

In vitro antioxidant activities of Med1 EPS were assayed against ABTS, H_2O_2, and FRAP compared with xanthan gum as standard (Fig. 12A-C). It showed significant free radical scavenging activity compared to standard xanthan gum. ABTS-mediated free radical scavenging activity was 94.23% at a low concentration of Med1 EPS (0.2 mg L^{-1}). However, the percentage of ABTS scavenging activity of Med1 EPS was found to be gradually decreased with increasing EPS concentration. Med1 EPS exhibited 33.89% H_2O_2-mediated free radical scavenging activity at similar concentrations. Maximum antioxidant activity for FRAP was ~82% at 5.0 mg L^{-1} Med1 EPS concentration. Whereas in case of FRAP-mediated antioxidant activity was found to be increased with increased EPS concentration.

Emulsifying activity study

In the present study, the emulsification activity of Med1 EPS was compared with commercially available bacterial biopolymer xanthan gum (Merck) against different vegetative oils (Fig. 12D). Med1 EPS had shown the highest emulsification activity against sunflower oil, 62.96%, with an EPS concentration of 0.05%, whereas activity was 53.57% at a concentration of 1% of EPS. For every vegetative oil, the emulsification activity was found to be less or similar at 1% EPS concentration compared to 0.5% EPS concentration (Fig. 12D). Only in the case of olive oil, the emulsification activity was a little higher (50%) in higher EPS concentration (1%) compared to lower EPS concentration of 0.5% (48.15%).

Flocculation activity determination

The flocculation activity was done using kaolin clay, represented in Fig. 12E. The flocculation activity had been gradually increased to 80 mg L^{-1}, after which no flocculation activity had been observed with increased EPS concentration. A similar kind of activity also had been observed for xanthan gum, where flocculation activity was found to increase gradually up to 60 mg L^{-1}, after which flocculation activity was found to decrease along with increased EPS concentration. The highest % flocculation of 33.9 was observed with 60 mg L^{-1} EPS concentration, while the lowest was 0% (100 mg L^{-1}).

Water retention and oil holding capacity

The isolated EPS had shown 107.6% water retention capacity (WHC) compared to control xanthan gum (183.3%). Along with water retention, oil holding capacity (OHC) is also an important property for use of EPS for biotechnological applications. For the presently isolated Med1 EPS, OHC was 110.8%, nearly similar to control xanthan gum (111.0%). According to the ANOVA analysis, significant statistical difference ($p < 0.05$) had been observed with control xanthan gum, presenting nearly similar capacity.

Discussion

Several works was documented from Chile like Northern Chilean Altiplano[59], Patagonia in the southern Chilean part[60–63] in terms of microbial diversity. However, the Central Andean Mountain region is rich in extreme environments, but very little has been explored regarding microbial biotechnology. Medano is a hot water spring in a stratovolcanic field, Laguna del Maule. However, Medano, aknown tourist spot, has a lower temperature than other hot water springs reported before in the same volcanic field by our group[8,11]. Several active and non-active volcanoes are near to the study site that are located in the Central Andean region. The present study site, hot spring Medano, had a nearly neutral pH (7.10 ± 0.07). The study site is rich in metals (Al, Cu, Mg, Mn, Ni,

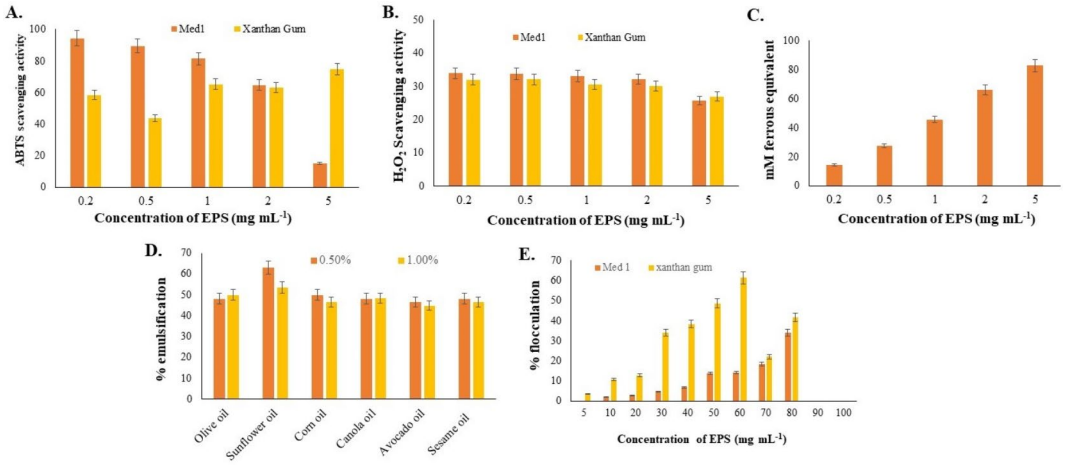

Fig. 12. In vitro antioxidant capability of the EPS produced by *Pseudomonas alcaligenes* Med1; where (A) ABTS radical scavenging activity; (B) H_2O_2 radical scavenging activity; (C) Ferric reducing ability (D) Emulsification activity against different food grade vegetative oil of the EPS and (E) Bioflocculation activity *Pseudomonas alcaligenes* Med1.

Pb, Zn, As). Presence of sulfate (SO_4^{2-}): 116.8 ± 4.8 mg L^{-1} and fluoride (F^-): 1.2 ± 0.0 mg L^{-1} indicate magnetic volatiles in the water due to meteoric water circulation in volcanic thermal water of the hot spring[61,64]. Microbiota inhabiting in this thermal fluid are in exposure to multiple extreme factors, like temperature, pH, presence of metals, and salinity. Chile has always been used as model site to understand the extreme environmental conditions[59,65]. In central Chile, the hot springs of the Maule region are comparatively underexplored in terms of biotechnological aspects of value-added bioactive compounds produced by the bacteria as a part of their stress resistance. The present study focuses on one of the extreme environments of the Maule region to understand bacterial life forms along with bacterial bioactive compounds.

The present study focuses on the isolation of EPS-producing bacterial strains from this unexplored extreme environment, a hot spring, Medano. Biofilm, organized to aggregate microorganisms within it, plays an essential role in survival under extreme conditions. Biofilm is an excellent bioactive component with structural complexity, which can be a future potential element for biotechnological use. Hence, our present study explored the EPS from thermotolerant *P. alcaligenes* Med1 showing bioactivity for future usage as food additive. Isolated bacteria had been identified in terms of whole genome sequencing to confirm the polysaccharide production in genomic level. Digital DNA-DNA hybridization, analysis of orthologous gene, determination of ANI value, and gene relatedness confirm the identification of the presently studied strain as *P. alcaligenes* Med1. Donor sugar in the reaction with glycosyltransferase usually found to be activated in the form of nucleoside diphosphate sugars, such as UDP-Glucose, or UDP-Galactose[66]. The presence of putative glycosyltransferase in the Med1 genome also indicates the polysaccharide synthesis by the isolated strain.

Cellulose-based exopolysaccharides have been reported previously from different species of *Pseudomonas*[67]. However, EPS from *P. alcaligenes* in extreme environments has yet to be reported. *Pseudomonas* is a γ-proteobacteria and versatile in nature, reported from different kinds of environments. Isolated thermotolerant *P. alcaligenes* Med1 in this study optimally produce ~ 6.8 g L^{-1} EPS at 37 °C temperature in the presence of carbon source (30 g L^{-1}) and nitrogen source (30 g L^{-1}). According to another previous report, *P. aeruginosa* G1 and *P. putida* G12 isolated from other sites have shown 192 mg L^{-1} and 182 mg L^{-1}, respectively, in the presence of various carbon sources, namely glucose, mannose, fructose[68]. *Pseudomonas* sp. PFAB4 isolated from an Indian hot spring produced 2.63 g L^{-1} EPS[69]. It can be seen that the yield of EPS from presently isolated bacteria is much higher compared to some other *Pseudomonas* sp. reported before. The developed optimization model can be generalized for EPS production by *P. alcaligenes* Med1 under the same conditions. From the ramp chart (Fig. 8), it may be observed that the desirability score of the optimization model is 0.942. Our study is the first report to characterize the EPS from *P. alcaligenes* isolated from a hot spring. However, the fitness model examining the determination coefficient (R^2) was documented before for other *Pseudomonas* species; for *Pseudomonas fluorescens* CrN6, R^2 was 0.9752 [70]; and for *Pseudomonas fluorescens* PGM37, R^2 was 0.9537 [71]. In our result, R^2 was 0.96 for *P. alcaligenes* Med1. Therefore, the strain we studied showed an excellent aggregate result when we compared the desirability model with different *Pseudomonas*. The best conditions achieved from the optimization experiment were used for further purification, characterization, and bioactivity studies.

Morphologically, Med1 EPS was found to be amorphous, non-porous, and compact in nature. This confirms the formation of film-like biopolymeric structure[72]. Interestingly, the biopolymer composed of carbon and oxygen as only key non-metal element. The monosaccharide composition analysis obtained by HPLC suggest Med1 EPS is a heteropolysaccharide with three different kind of monosaccharides like mannose, glucose, and galactose in a ratio of 10:3:0.3. FTIR spectrum confirm the presence of sugar units of mannose in α-anomeric configuration. The 1D and 2D-NMR analysis also supports this linkage in EPS, but also different glycosylic linkages. Med1 EPS is a heteropolysaccharide having the backbone made up of firstly [→1)-α-Manp-(2→] (A1) and [→1)-α-Manp-(3→] (B1) and second predominant linkage between the [→1)-α-Glcp-(3→] (E1) and [→1)-α-Glcp-(2→] (F1). This result indicates that there is more than one type of linkage in the EPS backbone or branching. Then, NMR analysis indicates that Med1 EPS could be a new galactoglucomannan type of EPS consist of principally mannose followed by glucose and galactose. In addition, a whole genome of the Med1 also confirms the compositional structure of EPS from a genomic point of view by indicating the presence of UDP-Glucose, UDP-Galactose. Before this kind of EPS was reported by *Pseudozyma* sp. SY16, a mannosylerythritol lipid-producing yeast[73]. There is a report on the thermophilic bacteria *Geobacillus* sp. strains WSUCF1 to produce a bioactive glucomannan type of EPS[6]. However, according to our knowledge, galactoglucomannan kind of EPS has not been reported from any species of *Pseudomonas* to date. The TGA analysis suggest this is a highly thermostable polysaccharide, which is useful for several applications in food industry. Moreover, thermal stability of Med1 EPS seems to be similar of EPS from *Pseudomonas stutzeri*, which showed a higher decomposition rate peaking at 291 °C, corresponding to their decomposition and pyrolysis[74] (Fig. 11D). Also, Med1 seems to have higher thermal stability than other studied *Pseudomonas* EPS (small endothermic peak at 83.0 °C followed by a strong exothermic peak at 314.2 °C). Such difference could be related to their different chemical structure. According to this data, Med1 EPS may be employed for functionalization and other chemical modification to expand its future potential application.

Extremophilic bacteria were found to be mostly non-pathogenic in nature, along with different bioactivity, making them suitable candidates for industrial use[8]. As per one example, a microbial heteropolysaccharide gellan extracted from extremophilic *Geobacillus stearothermophilus* reported to be used as a gelling substance and suspending agent in the food industry[75]. Hence, after analyzing the structural complexity in this study, EPS was also analyzed for in vitro activities to determine its efficacy as an industrially valuable compound for future sustainability. Med1 EPS has been found to have good antioxidant, flocculation, and emulsification properties.

Regarding the bioactivity (antioxidant properties ABTS, H_2O_2, and FRAP), the *P. alcaligenes* Med1 EPS showed concentration-dependent free radical scavenging activity as found before[8,11]. In the case of the ABTS method, dose-dependent antioxidant activity, ~ 94 – 15% scavenging activity at 0.2-5.0 mg L^{-1} EPS concentration. Here, the antioxidant concentration was found to be decreased with increased EPS concentration. However, the trend

was opposite for the control in this experiment, xanthan gum. In FRAP activity, the antioxidant activity was high (82.57%) at a higher concentration of EPS (5.0 mg L^{-1}). Thermophilic EPS creates an environment around the cell to protect it against free radicles produced due to extreme environmental conditions[76]. Antioxidant activity is an interesting property that improves the self-life of food, as it inhibits the oxidation of nutrients and vitamins during food storage[77]. Both free radical scavenging activity and metal ion chelation has been performed in this study to have an inclusive idea on the antioxidant potential of the EPS. Thus, Med1 EPS, with good antioxidant capacity, can be used as an antioxidant additive in the food industry. The Med1 EPS showed good emulsification activity against food-grade vegetable oils. Galactoglucomannan has been reported to have excellent emulsification activity and stabilize oil-in-water emulsion[78]. Structurally, the EPS has an extensive network that helps to form a continuous phase to stabilize the emulsion[79]. In food industries such as beverage, dairy, and meat processing, emulsion is an important factor. The food industry demands EPS with good emulsion properties for as thickening agent, developing macromolecular blocks between dispersed droplets in the aqueous phase[80]. Med1 EPS also has stable flocculation activity at lower EPS concentration (60 mg L^{-1}) due to having a neutral macromolecular structure associated with charged groups with probable traces of remaining proteins. At high concentrations, the viscosity of EPS solution is probably responsible for the blockage of active sites, which reduces the flocculation capacity[81], as similarly found in another study also[82]. Flocculation activity makes an EPS desirable for the easy separation of cells from the products for use in the food industry[83]. WHC is highly influenced by molecular weight, ionic form, and chemical composition of polysaccharides. Presently studied Med1 EPS showed 107.6% WHC, which is higher than other studied bacterial EPS, like ~ 98% WHC for *Bacillus licheniformis* EPS[84]. Though there are reports of high WHC for polysaccharides from animal sources, like chitosan from crab (138%) and shrimp (358%)[85], our studied EPS showed good WHC properties. WHC and OHC are important factors in the food industry, for example, to improve the crispness of chips, crackers, or snacks, to add texture to low moisture-baked food, etc[8]. Med1 EPS also demonstrates a good OHC (110.8%) compared to other studied bacterial EPS (*Lactobacillus* EPS only with OHC of 5.1%)[86]. Although chemical composition plays an important role in the OHC, the biopolymer's porosity and affinity with the oil also contribute to the activity. However, along with chemical composition, porosity and affinity with oil play important roles in the determination of the OHC of EPS and contribute to the bioactivity[8]. Therefore, EPS produced by *P. alcaligenes* Med1 presents good results with the possibility of being used as a food additive in the food industry.

In the present study, the physical and chemical structure of EPS produced by an unexplored Chilean hot water spring-inhabiting thermotolerant *P. alcaligenes* Med1 was thoroughly studied. To support the EPS production by genomic study, the whole genome of the isolated bacteria has also been explored. Even EPS production by *P. alcaligenes* Med1 had been optimized by CCD design of response surface methodology (RSM) to understand the effect of different factors separately, carbon source, nitrogen source, pH of the media, and bacterial concentration on EPS production. The EPS was only composed of carbon and oxygen, which had glucose, galactose, and mannose. Along with significant antioxidant, flocculation, and emulsification activity, Med1 EPS also exhibited good water retention capacity. From the result, it has been hypothesized that EPS might help in aggregating cells by forming a biofilm under stressful conditions that might help in cell-to-cell communication. Moreover, adhesion between the bacterial cells inside the biofilm with the cohesion of EPS is a part of bacterial survival strategy, along with water retention capacity to help the bacterial cells survive in extreme environmental stress, which also provides tolerance to host defense or other antimicrobial agents. According to our knowledge, the present study is the first one to highlight a functional EPS produced by *P. alcaligenes* Med1 isolated from a hot spring located in Central Andean Mountains of Chile.

Methods

Sample collection from Medano hot spring

Water samples were collected from the Medano hot spring, located at the Central Andean Mountains of Chile in the Maule region (-35.5733, -70.7785) in capped sterile bottles nearly 50 cm depth from the hot spring and used for isolation of thermotolerant EPS-producing bacteria. The physiochemical properties of water sample, such as temperature, pH, color, and conductivity, had been measured to synchronize the isolation and growth of the thermotolerant EPS-producing bacteria by using a multiparameter equipment (LAQUA PH120-K, HORIBA, Kyoto, Japan).

The collected water sample was filtered by using a polycarbonate filter with 0.45 µm porosity to analyze the physicochemical properties according to the Standard Methods for the Examination of Water and Wastewater as described by INN-Chile[87–89]. Required reagents (Suprapure, Merck, Darmstadt, Germany) were of high purity. Other physicochemical parameters like dissolved oxygen (DO), biochemical oxygen demand (BOD), total dissolved solids (TDS), total alkalinity, chlorides, color, turbidity, sulfates, nitrates, and sulfates of the collected water sample were determined. For the determination of dissolved oxygen, the Winkler method was used as described in Standard Methods for the Examination of Water and Wastewater[90]. Considering the geographical location of the Medano hot spring, located in the Southern Volcanic Zone, part of the Andean Volcanic Belt, the concentration metals such as iron (Fe), copper (Cu), aluminum (Al), magnesium (Mg), chromium (Cr), cadmium (Cd), manganese (Mn), nickel (Ni), lead (Pb), zinc (Zn), mercury (Hg), arsenic (As) and selenium (Se) determined as described by Fierro et al.,[91] and Banerjee et al.,[8]. The determinations of Fe, Cu, Al, Mg, Cr, Cd, Mn, Ni, Pb and Zn were carried out by atomic absorption spectroscopy with a flame technique. For the determination of Hg, the cold vapor technique was used and for As and Se, the hydride evolution technique was used. The spectrophotometer used was a Thermo Fisher Scientific ICE 3000 Series (Cambridge, United Kingdom).

Isolation and identification of EPS producing thermotolerant bacteria

The collected water sample was serially diluted (50 µL of each dilution) and aseptically inoculated in nutrient agar (NA) (Difco) media (pH 7.10). As the surface water temperature of the hot spring was observed to be 39.1 °C at the time of sample collection, thus for synchronization, the inoculated media was incubated at 37 °C for bacterial growth. However, in order to check the thermostability, bacterial isolate was screened for temperature tolerance under a range of temperature (10–60 °C). After 24 h of incubation, a yellowish transparent, convex, and mucoid colony of Med1 was chosen for EPS production according to the procedure described before by Banerjee et al.,[8]. Taxonomic identification of the isolate mucoid bacterial strain has been done following the recent study by Marín-Sanhueza et al.,[92] with slight modifications. Briefly, the 16 S rRNA region was amplified from isolated bacterial DNA with the universal 27 F and 1492R primers[93]. The obtained amplicons were sequenced, and EzTaxon has been used for identification (https://www.ezbiocloud.net/identify; Accessed January 10, 2022). Evolutionary distances between the sequences were calculated according to the method described by Tamura and Nei[94], and the phylogenetic tree was prepared following the maximum likelihood method using MEGA 7.0 [95], followed by deposition of the sequence in GenBank.

Whole genome sequencing, assembly, and annotation

Genomic DNA isolation and genome sequencing

Genomic DNA (gDNA) was isolated from a full-grown culture of *P. alcaligenes* strain Med1 using ZymoBiomics DNA/RNA miniprep kit (Zymo Research) according to the manufacturer's instructions. The gDNA concentration and quality (OD260/280 = 1.8~2.0) were assessed using Nanodrop 1000 (Thermo Fisher Technologies) and Qubit 4.0 (Thermo Fisher Technlogies). The gDNA was also checked on 0.7% agarose gel electrophoresis for high molecular size along with Lambda DNA HindIII cut DNA marker for 5 h at 40 Volts and gel image was documented by a Gel-documentation system (Gel Doc SR + System, Bio-Rad). The gDNA was sequenced using Oxford-Nanopore single molecule real-time sequencing technology (ONT-SMRT) at the Meta-Omics Lab facility of South Dakota Mines (SDSMT), Rapid City, SD, USA. High-quality 1.0 µg gDNA was processed for library preparation using a ligation sequencing kit (SQK-LSK109), as recommended (DNA damage repair and end-repair/dA tailing, adapter ligation) by Oxford-Nanopore. The sequencing library was purified three times with AMPureXP beads (Beckman Coulter Genomics, MA, United States) as per the Oxford-Nanopore library preparation recommendation for capturing of desired library fragment size (~10 kb) for sequencing. The final library was quantified on Qubit 4.0 and 100fmol of library was loaded with sequencing loading beads in the sequencing flow cell (R9.4.1) following standard procedures. The flow cell was placed on MinION sequencer and sequencing was achieved by 12-hour sequencing run with MinKNOW v22.03.6 (https://nanoporetech.com/news/news-introducing-new-minknow-app) with super accuracy base call option using Guppy v6.0.7 [96] (https://bio.tools/guppy).

The quality passed raw sequence data generated from Nanopore sequencing was further processed to assemble reads to generate a chromosome-level genome assembly. The super high-quality reads were assembled using Flye v2.8.3 [97] (https://github.com/mikolmogorov/Flye) with 3 iterations of Minimap2 v2.24 [98] (https://github.com/lh3/minimap2) for polishing. An extra polishing step was performed to achieve high-quality genome assembly, using Medaka v1.6.0 with default parameters (https://github.com/nanoporetech/medaka). The final polished and finished genome assembly was processed for further characterization and annotation. The genome completeness and quality were estimated using CheckM v1 [99] (https://github.com/Ecogenomics/CheckM). Gene prediction and annotation were achieved by Prokka v1.8 [100] (http://vicbioinformatics.com/) using ab initio algorithm Prodigal v2.6.3 for gene prediction and genus-specific for annotation (https://github.com/hyattpd/Prodigal). Prediction of tRNA, rRNAs, and CRISPR was done by Aragorn v1.2.41 [101] (https://anaconda.org/bioconda/aragorn), Barrnap v0.9 [100] (https://github.com/tseemann/barrnap), and MinCED v.4.2 [8] (https://github.com/ctSkennerton/minced) respectively. Genome annotation files were uploaded to the Proksee server[102] (https://proksee.ca/) to prepare a Circular genome map of strain Med1.

Strain identification and comparative genomics analysis

For taxonomic identification, type (Strain) Genome Server (TYGS) (https://tygs.dsmz.de/) was used where digital DNA: DNA hybridization (dDDH) values were calculated to identify closet type strain (Meier-Kolthoff and Göker, 2019). The genus and species level identification were studied by BLAST-based average nucleotide identity (ANIb) using the JSpeciesWS server (https://jspecies.ribohost.com/jspecieswsl/), and Average nucleotide identity (ANI) values were also calculated[103]. The 16 S rRNA gene obtained from the Med1 genome was compared with available sequences of cultured species on the EzBioCloud server[104] (https://www.ezbiocloud.net/). The phylogenetic tree of the 16 S rRNA gene was constructed using MEGA version 7.0 [105].

Based on digital DNA: DNA hybridization (dDDH) in the TYGS server, the three most closely related genomes have been chosen. The three closest strains (based on ANI) to Med1, (1) *Pseudomonas alcaligenes* NBRC 14,159, (2) *Pseudomonas subflava* YIM B01952 and (3) *Pseudomonas paralcaligenes* MRCP1333 were used for comparative genomic analysis. The genome sequences were downloaded from the European nucleotide archive (ENA) (https://www.ebi.ac.uk/ena/browser/search) database in FASTA format.

Determination of OrthoANI and Heat Map Study

ANI analysis was performed using the OAT tool (Orthologous Average Nucleotide Identity Tool) to establish relatedness between different strains (https://www.ezbiocloud.net/tools/orthoani). OAT determined the overall similarity between the two genome sequences. Unlike the original ANI algorithm, OrthoANI results in identical reciprocal similarities. However, for both OrthoANI and original ANI, the cut-off is 95–96% for species delineation[13]. A comparative heat map of strain Med1 with these three closely related sequences was prepared using OAT[13].

Subsystem gene categorization, and identification of unique genes
An open-source prokaryotic genome annotation system Rapid annotation System Technology (RAST) pipeline (https://rast.nmpdr.org/rast.cgi) was used for subsystem assignment to *P. alcaligenes* Med1. The visualization of the functionally annotated genome was done using SEED Viewer and the subsystem features were using the RAST pipeline[105].

To identify genes related to prophage, the PHAge Search Tool with Enhanced Sequence Translation (PHASTEST) web-based server (https://phastest.ca/) analyzed rapid identification and annotation of prophage sequence within the Med1 bacterial genome[17]. Genomic islands were predicted using IslandViewer4 [18] (https://www.pathogenomics.sfu.ca/islandviewer/).

Biosynthetic gene cluster analysis
To identify the biosynthetic gene cluster of the genome of the *P. alcaligenes* Med1 strain, the genome files (.fasta and .gff) were uploaded on antiSMASH v7.1.0[106] (https://antismash.secondarymetabolites.org) for the analysis.

Pan, core and accessory genome characteristics determination
Pangenomes helped to estimate the number of shared genes (core genome) and unique or variable genes (accessory genome) between the genomes. The Spine tool (a perl-based program) (http://spineagent.fsm.northwestern.edu/index_age.html) was used to analyze the core genome from selected genomes with ≥85% sequence identity as homologous[107]. AGEnt algorithm depends on a combination of the NUCmer function of the MUMmer software package v3.23 (https://mummer.sourceforge.net/) as well as the Perl script. An individual gene is considered to belong to an accessory genome if ≥50% of its sequence is located within the coordinates of an accessory region as a unique strain-specific region[24].

Optimization of media components for EPS production using response surface methodology (RSM)

Optimisation of EPS production by central composite design for P. alcaligenes Med1
The central composite design (CCD) with four different conditions, i.e. pH of media, bacterial concentration, carbon source and nitrogen source, was employed to study the optimization of EPS production. All the experimental setups were conducted for Med1 in a replicated of three to ensure adequacy. The highest, median, and lowest (+1, 0, -1 respectively) range was selected for different factors (Table 3). Complete designed matrix CCD for independent parameters with levels and actual, predicted response EPS are shown in Table 4. The designated flasks were inoculated and incubated at 37 °C temperature at 120 rpm for 4 days in a rotary shaker. The statistical analyses were carried out by the design expert software version 7.0; © Stat-Ease, Inc. (http://www.statease.com/dx7descr.html) to evaluate the effect of each parameter and their interaction to predict EPS production as described in the quadric optimization model (Eq. 2).

$$Y = \beta_0 + \sum_{i=1}^{k} \beta_0 x_i + \sum_{i=1}^{k} \beta_{ii} x_i^2 + \sum_{i=1}^{k-1} \sum_{i=2}^{k} \beta_{ij} x_i x_j \quad (2)$$

Where Y is the predicted response, β_0 is the intercept term, β_i is the linear effect, β_{ii} is the squared effect, β_{ij} is the interaction effect, and X_i and X_j are input variables that influence the response variable Y.

Validation of optimum conditions
Based on ANOVA analysis and optimization plot can be constructed by utilizing Design expert software to evaluate the optimum concentrations (carbon source g L^{-1}, nitrogen source g L^{-1}, PH, bacterial concentration ml L^{-1}) that maximize EPS production, briefly all independent parameters selected as in range mode and response EPS as maximize to develop ramp chart for optimization description. Optimum parameters obtained were validated in the laboratory to verify the predicted result of EPS production.

Physicochemical characterization of EPS

Morphological analysis (SEM-EDS and AFM)
Scanning electron microscopy (SEM) and Atomic force microscopy (AFM) were performed in order to understand the surface topography of the EPS with lyophilized sample. For SEM analysis, EPS was coated by gold using a Gold Sputter Coater (DII 29030SCTR Smart Coater) to make it conductive to observe under FESEM (JEOl-JSM 7610FPlus) at 15 kV accelerating voltage. Elemental composition i.e. compositional ratio of carbon/ nitrogen/ oxygen/ phosphorus/ sulfur of the isolated EPS was analyzed by energy dispersive X-ray spectroscopy (EDS) (X-Max-AZtec, Oxford Instruments) combined with FESEM (JEOl-JSM 7610FPlus). For AFM, 0.01 mg mL^{-1} EPS aqueous solution was prepared using Mili-Q water by doing vortex at room temperature. Approximately

Factor	Unit	Alpha	-1	0	1	Alpha
Carbon source	g L^{-1}	10	20	30	40	50
Nitrogen source	g L^{-1}	10	20	30	40	50
pH		6	7	8	9	10
Bacterial concentration	ml L^{-1}	10	20	30	40	50

Table 3. Experimental domin and levels of independent parameters for response surface methodology.

Std.	Run	Point type	Carbon source g L^{-1}	Nitrogen source g L^{-1}	pH	Bacterial concentration ml L^{-1}	EPS g L^{-1}	
							Actual	Predict
26	1	Center	30	30	8	30	3.1	3.15
5	2	Fact	20	20	9	20	1.67	1.89
29	3	Center	30	30	8	30	3.28	3.15
27	4	Center	30	30	8	30	3.26	3.15
22	5	Axial	30	30	10	30	0	0.2
9	6	Fact	20	20	7	40	6.5	6.3
24	7	Axial	30	30	8	50	3.64	3.54
28	8	Center	30	30	8	30	3	3.15
15	9	Fact	20	40	9	40	1.12	1.04
30	10	Center	30	30	8	30	3.19	3.15
3	11	Fact	20	40	7	20	3.42	3.52
19	12	Axial	30	10	8	30	3.19	3.09
23	13	Axial	30	30	8	10	3.24	3.16
21	14	Axial	30	30	6	30	6.83	6.85
1	15	Fact	20	20	7	20	6.5	6.45
18	16	Axial	50	30	8	30	2.81	2.72
17	17	Axial	10	30	8	30	3.67	3.58
14	18	Fact	40	20	9	40	0.81	0.77
11	19	Fact	20	40	7	40	3.6	3.82
20	20	Axial	30	50	8	30	1.1	1.04
25	21	Center	30	30	8	30	3.09	3.15
7	22	Fact	20	40	9	20	1	0.91
16	23	Fact	40	40	9	40	1.5	1.67
10	24	Fact	40	20	7	40	5	5.21
4	25	Fact	40	40	7	20	3.6	3.46
8	26	Fact	40	40	9	20	0.86	1.13
6	27	Fact	40	20	9	20	0.79	0.68
2	28	Fact	40	20	7	20	4.8	4.95
13	29	Fact	20	20	9	40	1.32	1.57
12	30	Fact	40	40	7	40	4.32	4.17

Table 4. Experimental design RSM based on CCD with actual and predicted response for EPS production.

5 µL of the EPS solution was drop casted on the cover slip and air dried. The surface images of the EPS were acquired by AFM microscope (diINNOVA, Bruker) at tapping mode of NanoDrive Innova system.

Monosaccharide composition analysis

Monosaccharide composition was analyzed by using high-pressure liquid chromatography (HPLC). For this, HPLC (Shimadzu, Kioto, Japan), attached with an LC-20AT Pump, a multiple autosampler (SIL-20 A) with a loop of 20 µL, a UV detector (SPD-20AV) within a range of 210 to 290 nm were used. A refractive index detector (RID-10 A) was connected to the equipment in series. Data were collected on a LabSolution software 1.25 Version system (Shimadzu, Kyoto, Japan) (https://www.shimadzu.com/an/products/software-informatics/software-option/labsolutions-cs/index.html). The analyses were performed with water at 0.8 mL min^{-1} and 65 °C with a 300 × 7.8 mm I.D. cation exchange column (Aminex HPX-87 H) equipped with a cation H^+ microguard cartridge (Bio-Rad Laboratories, Hercules, CA). Sugar standards were supplied by Sigma Chile. Different calibration curves of monosaccharides, namely glucose, galactose, and mannose, were used as a standard for quantification with a sugar concentration range of 200 – 10,000 µg mL^{-1}. The calibration parameters obtained for each curve were: glucose (140x—6277, R^2 0.999), galactose (101x-9566, R^2 0.999) and mannose (147x-26559, R^2 0.997).

Determination of molecular weight

The molecular weight of the EPS from Med1 was determined by gel permeation chromatography (GPC) 1100 HPLC system (Agilent Technologies, Santa Clara, USA) attached to Shodex columns (40, 300, 1000) by maintaining specific conditions (10 µL, 0.1 g mL^{-1}; solvent 0.1 M sodium nitrate; $\Phi = 0.5$ mL min^{-1}; temperature = 50 °C). Pullulan, a commercial polysaccharide (Sigma, St. Louis, United States) was used as standard (0.3–700 kDa).

Thermogravimetric analysis
Thermogravimetric analysis was done using a thermogravimetric analyzer (TGA) Cahn-Ventron 2000 (Cahn Scientific, Irvine, CA, USA) equipped with a microprocessor driven temperature control unit and a thermal analysis data station to determine the thermal stability of Med1 EPS. About 5 mg of crude lyophilized EPS was placed on an aluminum sample pan with a temperature raising range from 25 to 600 °C under a nitrogen atmosphere with an N_2 gas flow of 50 mL min^{-1} using alumina as a control at a heating rate of 10 °C min^{-1}.

Fourier transform infrared (FTIR) Spectroscopy analysis
The functional group differential pattern was identified and analyzed by Fourier transform infrared (FTIR)[8]. The molecular curve produced by purified EPS of Med1 was analyzed by the FTIR spectrum ranging from 500 cm^{-1} to 4000 cm^{-1} at 64 scans, at a resolution of 4 cm^{-1}. FTIR sample was prepared by KBr pellet method at 1:90 ratio. Then it was directly exposed to the FTIR spectrometer (Jasco-4000, Jasco Analytical Spain, Spain) for the interpretation of different spectral range to identify the functional group. Final data was processed through OriginPro 8 software (https://www.originlab.com/).

Nuclear magnetic resonance (NMR) spectroscopy analysis
The ^1H nuclear magnetic resonance analysis was performed as previously described by Banerjee et al.,[111] $^1H/^{13}C$ Multiplicity-Edited HSQC (HSQC)-NMR experiment was performed as previously described by[108–110]. Twenty milligrams of *P. alcaligenes* Med1 exopolysaccharide was analyzed with a 500 MHz NMR spectrometer (Bruker Biospin, Rheinstetten, Germany) with a triple resonance probe. The sample was re-suspended in 99.9% deuterium oxide (Cambridge Isotope Laboratory, Cambridge, MA), and the $^1H/^{13}C$ Multiplicity-Edited HSQC (HSQC) spectra were recorded with 1024 × 512 points and 256 scans using an Echo-Antiecho acquisition mode with globally optimized alternating phase rectangular pulses for decoupling at 35 °C. The spectra were processed using TopSpin 4.3.1 (Bruker Biospin) software (https://www.bruker.com/protected/en/services/software-downloads/nmr.html). The chemical shifts were manually compared to the Carbohydrate Structure Database (CSDB)[40] and to specific literature to attribute the glycosidic linkages. The $^1H/^{13}C$ HMBC (Heteronuclear Multiple Bond Correlation) spectra were recorded with 2048 × 200 points and 512 scans, taking a 50ms delay for the evolution of long-range couplings and set with no decoupling during the acquisition time. A low-pass filter and a QF magnitude acquisition mode were used[111].

Functional properties elucidation of the EPS

In vitro antioxidant activity determination
ABTS [2,2'-azino-bis (3-ethylbenzothiazolin-6-sulfonic acid)] radical scavenging activity was determined according to the method of Nitha et al.,[112] with minor modification. The ABTS solution was diluted in phosphate buffer (pH 7.40) to acquire an absorbance of ~0.75 at 734 nm. To prepare the reaction mixture, 180 µL of different EPS solutions of different concentrations (0.2, 0.5, 1, 2 and 5 mg mL^{-1}) was mixed with 20 µL of ABTS radical solution followed by a reaction for 5 min at 30 °C in the dark to generate free radicles. Mobi-Microplate Spectrophotometer (μ_2 MicroDigital, Seoul, South Korea) was used finally for recording the absorbance at 734 nm, followed by calculation to determine the percentage of ABTS scavenging activity using Eq. 3, where in this case, A_0 is the absorbance value of ABTS radical solution without the sample, and A_1 is the absorbance value of EPS solution. Xanthan gum has been used as the positive control.

The free radical scavenging activity of EPS against hydroxyl radical was estimated by performing H_2O_2 scavenging activity and has been determined according to the method described before by Ruch et al.,[113] with some modifications. A volume of 50 µL of EPS solution of different concentrations (0.2, 0.5, 1, 2 and 5 mg mL^{-1}) was added with 30 µL of H_2O_2 solution (40 mM) and 120 µL of phosphate buffer (0.1 M, pH 7.40). Then, the mixture was vigorously shaken, followed by incubation at 30 °C for 10 min. Then, the absorbance of the resulting reaction mixture was measured at 230 nm using a Mobi-Microplate Spectrophotometer (μ_2 MicroDigital, Seoul, South Korea). The percentage of H_2O_2 scavenging activity was calculated as follows (Eq. 3):

$$[1 - (A_1 - A_2)/A_0] \times 100 \tag{3}$$

Where A_0 is the absorbance of the control MiliQ water, A_1 is the absorbance of the sample, and A_2 is the absorbance of the sample without H_2O_2 solution. Xanthan gum has also been used as the positive control.

Ferric reducing Antioxidant Power Activity (FRAP) has been analyzed as described before by Benzie and Strain[114] with some modifications using the FRAP assay kit (BioVision, Mil Pitas, USA). 10 µL of EPS samples of different concentrations, i.e. 0.2, 0.5, 1, 2, and 5 mg mL^{-1}, was mixed with 19 µL of ferric chloride ($FeCl_3$), 152 µL of FRAP assay buffer and 19 µL of FRAP probe and incubated at 30 °C for 60 min in dark condition. Xanthan gum was used as a positive control. The calibration curve was calculated using different concentrations of ferrous standard provided in the kit. The absorbance of the mixture was measured at 594 nm in a Mobi-Microplate Spectrophotometer (µ2 MicroDigital, Seoul, South Korea), and FRAP activity was calculated using Eq. 4.

$$B \times D/V \tag{4}$$

Where B is the amount of ferrous ammonium sulfate from the standard curve (nmol), D is the dilution factor, and V is the volume of sample added to the reaction well (in µL).

Emulsifying activity study
Med1 EPS was examined for its emulsification activity against different food-grade vegetative oils, i.e. Coconut oil, Corn oil, Canola oil, Avocado oil, Sunflower oil, Olive oil, and Sesame oil according to the methodology

described before by Cooper and Goldenberg[115] with little modification. EPS solution was prepared at a concentration of 1 mg mL^{-1} and mixed with food-grade vegetative oils in a ratio of 2:3 (v/v). After 24 h of time reaction interval, oil, emulsion, and aqueous layers were measured to determine emulsion stability in terms of emulsification index (E_{24}) calculated by the Eq. 5.

$$[(\text{volume of the emulsion layer} \times \text{total volume}^{-1}) \times 100] \tag{5}$$

Being a most commonly and regularly used commercial bacterial EPS as an emulsifier, xanthan gum[116] was used as a control. Hence, xanthan gum (Sigma) as a commercially available natural standard and Tween 20 (Sigma) as a synthetic surfactant were used in this experiment to compare the emulsification activity of *P. alcaligenes* Med1 EPS.

Flocculation activity determination

The flocculation activity of the EPS was measured according to the method described before by Pu et al.,[117] with some modifications. Different concentration of EPS solution (10–100 mg L^{-1}) was added with 1% $CaCl_2$ containing kaolin suspension (pH 7.0, 4 g L^{-1}) in a 1:1 (v/v) ratio, stirred and kept unindentured for 10 min. Finally, the absorbance of the supernatant was measured at 550 nm using Mobi-Microplate Spectrophotometer (μ_2 MicroDigital, Seoul, South Korea). The percentage of flocculation was calculated by the Eq. 6:

$$[(A - B)/A] \times 100 \tag{6}$$

where A is the absorbance of the control supernatant, and B is the absorbance of the sample.

Water retention and oil holding capacity

The water-retention capacity (WHC) of the EPS produced by *P. alcaligenes* Med1 was measured using the methods reported by Kumari et al.,[85]. 500 mg of EPS was mixed with 10 mL of distilled water by using cyclomixer for 1 min. The solution was kept at 37 °C for 30 min with intermediate stirrings followed by centrifugation at 3200 rpm for 25 min. Finally, the supernatant was decanted after centrifugation to calculate the water-holding capacity (WHC) using the following formula (Eq. 7):

$$\%\,\text{WHC} = \text{Water bound weight (g)}/\text{Initial sample weight (g)} \times 100 \tag{7}$$

The oil-holding capacity (OHC) of the study Med1 EPS was calculated following the standard method used by Wang and Kinsella[118], with little modifications. 500 mg of lyophilized EPS was mixed with 10 mL of sunflower oil in a cyclomixer, and the mixture was kept for 30 min at 37 °C with intermediate shaking every 10 min. Finally, after centrifugation at 3200 rpm for 25 min, the supernatant was used to calculate Oil-holding capacity (OHC) using the following formula (Eq. 8):

$$\%\,\text{OHC} = \text{Oil bound weight (g)}/\text{Initial sample weight (g)} \times 100 \tag{8}$$

Data availability

Whole genome of Pseudomonas alcaligenes Med1 is available under the accession number CP154874 in NCBI GeneBank (https://www.ncbi.nlm.nih.gov/).

Received: 16 June 2024; Accepted: 30 September 2024
Published online: 23 October 2024

References

1. Carrizo, D., Sánchez-García, L. & Gómez, F. Molecular evidences of life in a poly-extreme environment in Ethiopia, the Dallol Hot Springs area, based on lipidic biomarkers. In *European Planetary Science Conference* EPSC2018–E2044 (2018).
2. Saxena, R. et al. Metagenomic analysis of Hot Springs in Central India reveals hydrocarbon degrading thermophiles and pathways essential for survival in extreme environments. *Front. Microbiol.* **7**, 2123. https://doi.org/10.3389/fmicb.2016.02123 (2017).
3. Casillo, A., Lanzetta, R., Parrilli, M. & Corsaro, M. M. Exopolysaccharides from marine and marine extremophilic bacteria: Structures, properties, ecological roles and applications. *Mar. Drugs* **16**(2), 69. https://doi.org/10.3390/md16020069 (2018).
4. Nichols, C. M. et al. Bacterial exopolysaccharides from extreme marine environments with special consideration of the Southern Ocean, sea ice, and deep-sea hydrothermal vents: A review. *Mar. Biotechnol.* **7**(4), 253–271. https://doi.org/10.1007/s10126-004-5118-2 (2005).
5. Salama, Y. et al. Characterization, structure, and function of extracellular polymeric substances (EPS) of microbial biofilm in biological wastewater treatment systems: A review. *Desalin. Water Treat.* **57**(35), 16220–16237. https://doi.org/10.1080/19443994.2015.1077739 (2016).
6. Wang, J., Salem, D. R. & Sani, R. K. Two new exopolysaccharides from a thermophilic bacterium Geobacillus sp. WSUCF1: Characterization and bioactivities. *New Biotechnol.* **61**, 29–39. https://doi.org/10.1016/j.nbt.2020.11.004 (2021).
7. Wang, J., Salem, D. R. & Sani, R. K. Extremophilic exopolysaccharides: A review and new perspectives on engineering strategies and applications. *Carbohydr. Polym.* **205**, 8–26. https://doi.org/10.1016/j.carbpol.2018.10.011 (2019).
8. Banerjee, A. et al. Optimization and characterization of a novel exopolysaccharide from *Bacillus haynesii* CamB6 for food applications. *Biomolecules.* **12**(6), 834. https://doi.org/10.3390/biom12060834 (2022).
9. Gan, L., Li, X., Wang, H., Peng, B. & Tian, Y. Structural characterization and functional evaluation of a novel exopolysaccharide from the moderate halophile *Gracilibacillus* sp. SCU50. *Int. J. Biol. Macromol.* **154**, 1140–1148. https://doi.org/10.1016/j.ijbiomac.2019.11.143 (2020).
10. Banerjee, A., Rudra, S. G., Mazumder, K., Nigam, V. & Bandopadhyay, R. Structural and functional properties of exopolysaccharide excreted by a novel *Bacillus anthracis* (strain PFAB2) of hot spring origin. *Indian J. Microbiol.* **58**(1), 39–50. https://doi.org/10.1007/s12088-017-0699-4 (2018).

11. Banerjee, S. et al. Characterization of Chilean hot spring-origin Staphylococcus sp. BSP3 produced exopolysaccharide as biological additive. *Nat. Prod. Bioprospecting*. **14**(1), 1–16. https://doi.org/10.1007/s13659-024-00436-0 (2024).
12. Yoon, S. H. et al. Introducing EzBioCloud: A taxonomically united database of 16S rRNA and whole genome assemblies. *Int. J. Syst. Evol. Microbiol.* **67**, 1613–1617. https://doi.org/10.1099/ijsem.0.001755 (2017).
13. Lee, I., Kim, O., Park, Y., Chun, J. & OrthoANI,. An improved algorithm and software for calculating average nucleotide identity. *Int. J. Syst. Evol. MicroBiol.* **66**(2), 1100–1103. https://doi.org/10.1099/ijsem.0.000760 (2016).
14. Boels, I. C. et al. Identification and functional characterization of the Lactococcus lactis rfb operon, required for dTDP-rhamnose biosynthesis. *J. Bacteriol.* **186**(5), 1239–1248 (2004).
15. Cuthbertson, L., Kos, V. & Whitfield, C. ABC transporters involved in export of cell surface glycoconjugates. *Microbiol. Mol. Biol. Rev. MMBR* **74**(3), 341–362. https://doi.org/10.1128/MMBR00009-10 (2010).
16. Acosta-Jurado, S. et al. Exopolysaccharide production by *Sinorhizobium fredii* HH103 is repressed by Genistein in a NodD1-Dependent manner. *PLoS ONE* **11**(8), e0160499. https://doi.org/10.1371/journal.pone.0160499 (2016).
17. Arndt, D., Marcu, A., Liang, Y. & Wishart, D. S. PHAST, PHASTER and PHASTEST: Tools for finding prophage in bacterial genomes. *Brief. Bioinform.* **20**(4), 1560–1567. https://doi.org/10.1093/bib/bbx121 (2019).
18. Bertelli, C. et al. IslandViewer 4: Expanded prediction of genomic islands for larger-scale datasets. *Nucleic Acids Res.* **45**(W1), W30–W35. https://doi.org/10.1093/nar/gkx343 (2017).
19. Chien, C. C., Huang, C. H. & Lin, Y. W. Characterization of a heavy metal translocating P-type ATPase gene from an environmental heavy metal resistance *Enterobacter* sp. isolate. *Appl. Biochem. Biotechnol.* **169**, 1837–1846. https://doi.org/10.1007/s12010-012-0047-4 (2013).
20. Audy, J., Labrie, S., Roy, D. & LaPointe, G. Sugar source modulates exopolysaccharide biosynthesis in *Bifidobacterium longum* subsp. Longum CRC 002. *Microbiology*. **156**(3), 653–664. https://doi.org/10.1099/mic.0.033720-0 (2010).
21. Paquette, S., Møller, B. L. & Bak, S. On the origin of family 1 plant glycosyltransferases. *Phytochemistry*. **62**(3), 399–413. https://doi.org/10.1016/S0031-9422(02)00558-7 (2003).
22. Safari, M., Yakhchali, B. & Shariati, J. Comprehensive genomic analysis of an indigenous Pseudomonas pseudoalcaligenes degrading phenolic compounds. *Sci. Rep.* **9**(1), 12736. https://doi.org/10.1038/s41598-019-49048-6 (2019).
23. Ozer, E. A. ClustAGE: A tool for clustering and distribution analysis of bacterial accessory genomic elements. *BMC Bioinform.* **19**, 150. https://doi.org/10.1186/s12859-018-2154-x (2018).
24. Ozer, E. A., Allen, J. P. & Hauser, A. R. Characterization of the core and accessory genomes of Pseudomonas aeruginosa using bioinformatic tools spine and AGEnt. *BMC Genom.* **15**, 1–17 (2014).
25. Kanmani, P. et al. Optimization of media components for enhanced production of *Streptococcus phocae* PI80 and its Bacteriocin using response surface methodology. *Braz J. Microbiol.* **42**, 716–720. https://doi.org/10.1590/S1517-83822011000200038 (2011).
26. Preetha, S. P., Kanniappan, M., Selvakumar, E., Nagaraj, M. & Varalakshmi, P. Lupeol ameliorates aflatoxin B1-induced peroxidative hepatic damage in rats. *Comp. Biochem. Physiol.* **143**, 333. https://doi.org/10.1016/j.cbpc.2006.03.008 (2006).
27. Breig, S. J. M. & Luti, K. J. K. Response surface methodology: A review on its applications and challenges in microbial cultures. *Mater. Today Proc.* **42**, 2277–2284. https://doi.org/10.1016/j.matpr.2020.12.316 (2021).
28. Mohammed, S. J. & Luti, K. J. K. A kinetic model for prodigiosin production by Serratia marcescens as a bio-colorant in bioreactor. In: AIP Conference Proceedings, vol 1. AIP Publishing LLC, Melville, p 020027, (2020).
29. Chen, Z. et al. Isolation of exopolysaccharide-producing bacteria and yeasts from Tibetan kefir and characterisation of the exopolysaccharides. *Int. J. Dairy Technol.* **69**, 410–417. https://doi.org/10.1111/1471-0307.12276 (2016).
30. Yadav, V., Prappulla, S. G., Jha, A. & Poonia, A. A novel exopolysaccharide from probiotic *Lactobacillus fermentum* CFR 2195: Production, purification and characterization. *Biotechnol. Bioinf. Bioeng.* **1**(4), 415–421 (2011).
31. Kanamarlapudi, S. L. R. K. & Muddada, S. Characterization of exopolysaccharide produced by *Streptococcus thermophilus* CC30. BioMed Res. Int. **2017,** (2017).
32. Pham, D. K., Ivanova, E. P., Wright, J. P. & Nicolau, D. V. AFM analysis of the extracellular polymeric substances (EPS) released during bacterial attachment on polymeric surfaces. In *Manipulation and Analysis of Biomolecules, Cells, and Tissues* 151–159 (SPIE, 2003).
33. Sabando, C. et al. Novel hydrocolloid film based on pectin, starch and Gunnera tinctoria and Ugni molinae plant extracts for wound dressing applications. *Curr. Top. Med. Chem.* **20**, 280–292. https://doi.org/10.2174/1568026620666200124100631 (2020).
34. Wang, L. et al. Structural characterization and bioactivity of exopolysaccharide synthesized by *Geobacillus* sp. TS3–9 isolated from radioactive radon hot spring. *Adv. Biotechnol. Microbiol.* https://doi.org/10.19080/AIBM.2017.04.555635 (2017).
35. Yu, L. et al. Preparation and partial structural characterization of the exopolysaccharide from *Bacillus mucilaginosus* SM-01. *Carbohyd. Polym.* **146**, 217–223. https://doi.org/10.1016/j.carbpol.2016.03.038 (2016).
36. Synytsya, A. & Novak, M. Structural analysis of glucans. *Ann. Transl. Med.* **2**, 17–31 (2014).
37. Chen, Y. et al. Structural characterization and antioxidant properties of an exopolysaccharide produced by the mangrove endophytic fungus aspergillus sp. Y16. *Bioresour. Technol.* **102**, 8179–8184. https://doi.org/10.1016/j.biortech.2011.06.048 (2011).
38. Jana, U. K. & Kango, N. Characteristics and bioactive properties of mannooligosaccharides derived from agro-waste mannans. *Int. J. Biol. Macromol.* **149**, 931–940. https://doi.org/10.1016/j.ijbiomac.2020.01.304 (2020).
39. Casillo, A. et al. Physicochemical approach to understanding the structure, conformation, and activity of mannan polysaccharides. *Biomacromolecules*. **22**(4), 1445–1457. https://doi.org/10.1021/acs.biomac.0c01659 (2021).
40. Toukach, P. V. & Egorova, K. S. Carbohydrate structure database merged from bacterial, archaeal, plant and fungal parts. *Nucleic Acids Res. - Database Issue*. **44(D1)**, D1229–D1236. https://doi.org/10.1093/nar/gkv840 (2016). (2016).
41. Toukach, P. V. & Egorova, K. S. Glycoinformatics Bacterial, plant, and fungal carbohydrate structure databases: Daily usage. 55–85, (2015). https://doi.org/10.1007/978-1-4939-2343-4_5
42. Bochkov, A. Y. & Toukach, P. V. CSDB/SNFG structure editor: An online glycan builder with 2D and 3D structure visualization. *J. Chem. Inf. Model.* **61**(10), 4940–4948. https://doi.org/10.1021/acs.jcim.1c00917 (2021).
43. Toukach, P. V. & Egorova, K. S. New features of Carbohydrate structure database notation (CSDB Linear), as compared to other carbohydrate notations. *J. Chem. Inf. Model.* **60**(3), 1276–1289. https://doi.org/10.1021/acs.jcim.9b00744 (2019).
44. Neelamegham, S. et al. Updates to the symbol nomenclature for glycans guidelines. *Glycobiology*. **29**(9), 620–624. https://doi.org/10.1093/glycob/cwz045 (2019).
45. Lewis, A. L. et al. Cataloging natural sialic acids and other nonulosonic acids (NulOs), and their representation using the symbol nomenclature for glycans. *Glycobiology*. **33**(2), 99–103. https://doi.org/10.1093/glycob/cwac072 (2023).
46. Ye, S. et al. Biosynthesis of selenium rich exopolysaccharide (Se-EPS) by *Pseudomonas* PT-8 and characterization of its antioxidant activities. *Carbohydr. Polym.* **142**, 230–239. https://doi.org/10.1016/j.carbpol.2016.01.058 (2016).
47. Ljpkind, G. M., Shashkov, A. S., Nifant'ev, N. E. & Kochetkov, N. K. Computer-assisted analysis of the structure of regular branched polysaccharides containing 2, 3-disubstituted rhamnopyranose and mannopyranose residues on the basis of 13 C NMR data. *Carbohydr. Res.* **237**, 11–22. https://doi.org/10.1016/S0008-6215(92)84229-L (1992).
48. Katzenellenbogen, E. et al. Structure of an abequose-containing O-polysaccharide from *Citrobacter freundii* O22 strain PCM 1555. *Carbohydr. Res.* **344**(13), 1724–1728. https://doi.org/10.1016/j.carres.2009.06.005 (2009).
49. Katzenellenbogen, E. et al. Structures of a unique O-polysaccharide of *Edwardsiella tarda* PCM 1153 containing an amide of galacturonic acid with 2-aminopropane-1, 3-diol and an abequose-containing O-polysaccharide shared by E. Tarda PCM 1145, PCM 1151 and PCM 1158. *Carbohydr. Res.* **355**, 56–62. https://doi.org/10.1016/j.carres.2012.04.004 (2012).

50. Van Calsteren, M. R., Pau-Roblot, C., Bégin, A. & Roy, D. Structure determination of the exopolysaccharide produced by *Lactobacillus rhamnosus* strains RW-9595 M and R. *Biochem. J.* **363** (1), 7–17. https://doi.org/10.1042/bj3630007 (2002).
51. Zdorovenko, E. L. et al. Structure of the cell wall polysaccharides of probiotic bifidobacteria Bifidobacteriumbifidum BIM B-465. *Carbohydr. Res.* **344**(17), 2417–2420. https://doi.org/10.1016/j.carres.2009.08.039 (2009).
52. Vinogradov, E. V., Bock, K., Petersen, B. O., Holst, O. & Brade, H. The structure of the carbohydrate backbone of the lipopolysaccharide from *Acinetobacter* strain ATCC 17905. *Eur. J. Biochem.* **243**(1-2), 122–127. https://doi.org/10.1046/j.1432-1327.2001.02047.x (1997).
53. Vinogradov, E., Cedzynski, M., Ziolkowski, A. & Swierzko, A. The structure of the core region of the lipopolysaccharide from Klebsiella pneumoniae O3: 3-Deoxy-α-D-manno-octulosonic acid (α-Kdo) residue in the outer part of the core, a common structural element of Klebsiella pneumoniae O1, O2, O3, O4, O5, O8, and O12 lipopolysaccharides. *Eur. J. Biochem.* **268**(6), 1722–1729. https://doi.org/10.1046/j.1432-1327.2001.02047.x (2001).
54. Bystrova, O. V. et al. Structural studies on the core and the O-polysaccharide repeating unit of *Pseudomonas aeruginosa* immunotype 1 lipopolysaccharide. *Eur. J. Biochem.* **269**(8), 2194–2203. https://doi.org/10.1046/j.1432-1033.2002.02875.x (2002).
55. Vinogradov, E. & Sidorczyk, Z. The structure of the carbohydrate backbone of the rough type lipopolysaccharides from *Proteus penneri* strains 12, 13, 37 and 44. *Carbohydr. Res.* **337**(9), 835–840. https://doi.org/10.1016/S0008-6215(02)00037-X (2002).
56. Galbraith, L., George, R., Wyklicky, J. & Wilkinson, S. G. Structure of the O-specific polysaccharide from *Bukholderia pickettii* strain NCTC 11149. *Carbohydr. Res.* **282**(2), 263–269. https://doi.org/10.1016/0008-6215(95)00387-8 (1996).
57. Vinogradov, E., Perry, M. B. & Conlan, J. W. Structural analysis of *Francisella tularensis* lipopolysaccharide. *Eur. J. Biochem.* **269**(24), 6112–6118. https://doi.org/10.1046/j.1432-1033.2002.03321.x (2002).
58. Lu, L., Gu, G., Xiao, M. & Wang, F. Separation and structure analysis of trisaccharide isomers produced from lactose by *Lactobacillus bulgaricus* L3 β-galactosidase. *Food Chem.* **121**(4), 1283–1288. https://doi.org/10.1016/j.foodchem.2010.01.050 (2010).
59. Zhang, Q. et al. Composition and predicted functions of the bacterial community in spouting pool sediments from the El Tatio Geyser field in Chile. *Arch. Microbiol.* **203**, 389–397. https://doi.org/10.1007/s00203-020-02020-9 (2021).
60. Mackenzie, R., Pedrós-Alió, C. & Díez, B. Bacterial composition of microbial mats in Hot Springs in Northern Patagonia: Variations with seasons and temperature. *Extremophiles* **17**, 123–136. https://doi.org/10.1007/s00792-012-0499-z (2013).
61. Cordell, D., Unsworth, M. J. & Díaz, D. Imaging the Laguna Del Maule Volcanic Field, central Chile using magnetotellurics: Evidence for crustal melt regions laterally-offset from surface vents and lava flows. *Earth Planet. Sci. Lett.* **488**, 168–180. https://doi.org/10.1016/j.epsl.2018.01.007 (2018).
62. Lavergne, C. et al. Temperature differently affected methanogenic pathways and microbial communities in sub-antarctic freshwater ecosystems. *Environ. Int.* **154**, 106575. https://doi.org/10.1016/j.envint.2021.106575 (2021).
63. Maturana-Martínez, C., Fernández, C., González, H. E. & Galand, P. E. Different active Microbial communities in two contrasted subantarctic fjords. *Front. Microbiol.* **12**, 1592. https://doi.org/10.3389/fmicb.2021.620220 (2021).
64. Taran, Y. & Kalacheva, E. Acid sulfate-chloride volcanic waters; formation and potential for monitoring of volcanic activity. *J. Volcanol Geotherm. Res.* **405**, 107036. https://doi.org/10.1016/j.jvolgeores.2020.107036 (2020).
65. Alcamán-Arias, M. E. et al. Diurnal changes in active carbon and nitrogen pathways along the temperature gradient in Porcelana hot spring microbial mat. *Front. Microbiol.* **9**, 2353. https://doi.org/10.3389/fmicb.2018.02353 (2018).
66. Wang, G., Li, J., Xie, S., Zhai, Z. & Hao, Y. The N-terminal domain of rhamnosyltransferase EpsF influences exopolysaccharide chain length determination in Streptococcus thermophilus 05–34. *PeerJ*. **8**, e8524. https://doi.org/10.7717/peerj.8524 (2020).
67. Heredia-Ponce, Z. et al. Biological role of EPS from Pseudomonas syringae Pv. Syringae UMAF0158 extracellular matrix, focusing on a psl-like polysaccharide. *Npj Biofilms Microbiomes*. **6**(1), 37 (2020).
68. Celik, G. Y., Aslim, B. & Beyatli, Y. Characterization and production of the exopolysaccharide (EPS) from *Pseudomonas aeruginosa* G1 and *Pseudomonas putida* G12 strains. *Carbohydr. Polym.* **73**(1), 178–182. https://doi.org/10.1016/j.carbpol.2007.11.021 (2008).
69. Banerjee, A. et al. Characterization of exopolysaccharide produced by *Pseudomonas* sp. PFAB4 for synthesis of EPS-coated AgNPs with antimicrobial properties. *J. Environ. Polym. Degrad.* **28**, 242–256. https://doi.org/10.1007/s10924-019-01602-z (2020).
70. Sirajunnisa, A. R., Vijayagopal, V., Sivaprakash, B., Viruthagiri, T. & Surendhiran, D. Optimization, kinetics and antioxidant activity of exopolysaccharide produced from rhizosphere isolate, *Pseudomonas fluorescens* CrN6. *Carbohydr. Polym.* **135**, 35–43. https://doi.org/10.1016/j.carbpol.2015.08.080 (2016).
71. Okoro, O. V., Gholipour, A. R., Sedighi, F., Shavandi, A. & Hamidi, M. Optimization of Exopolysaccharide (EPS) production by *Rhodotorula mucilaginosa* sp. GUMS16. *Chem. Eng.* **5**(3), 39. https://doi.org/10.3390/chemengineering5030039 (2021).
72. Feng, F. et al. Characterization of highly branched dextran produced by *Leuconostoc citreum* B-2 from pineapple fermented product. *Int. J. Biol. Macromol.* **113**, 45–50. https://doi.org/10.1016/j.ijbiomac.2018.02.119 (2018).
73. Kim, K. N. et al. A novel galactoglucomannan exopolysaccharide produced by oil fermentation with *Pseudozyma* sp. SY16. *Biotechnol. Bioprocess Eng.* **25**, 742–748. https://doi.org/10.1007/s12257-020-0066-x (2020).
74. Meena, S. V. K. M., Tripathi, A. D. & Ts, R. L. Optimization and characterization of alginic acid synthesized from a novel strain of *Pseudomonas stutzeri*. *Biotechnol. Rep.* **27**, e00517. https://doi.org/10.1016/j.btre.2020.e00517 (2020).
75. Kambourova, M. et al. Production and characterization of a microbial glucan, synthesized by *Geobacillus tepidamans* V264 isolated from Bulgarian hot spring. *Carbohydr. Polym.* **77**(2), 338–343. https://doi.org/10.1016/j.carbpol.2009.01.004 (2009).
76. Su, Y. & Li, L. Structural characterization and antioxidant activity of polysaccharide from four Auriculariales. *Carbohydr. Polym.* **229**, 115407. https://doi.org/10.1016/j.carbpol.2019.115407 (2019).
77. Leyva-Porras, C., Román-Aguirre, M., Cruz-Alcantar, P., Pérez-Urizar, J. T. & dora-Leos, M. Z. Application of antioxidants as an alternative improving of shelf life in foods. *Polysaccharides*. **2**, 594–607. https://doi.org/10.3390/polysaccharides2030036 (2021).
78. Zhao, H., Mikkonen, K. S., Kilpeläinen, P. O. & Lehtonen, M. I. Spruce galactoglucomannan-stabilized emulsions enhance bioaccessibility of bioactive compounds. *Foods*. **9**(5), 672. https://doi.org/10.3390/foods9050672 (2020).
79. Song, B., Zhu, W., Song, R., Yan, F. & Wang, Y. Exopolysaccharide from *Bacillus vallismortis* WF4 as an emulsifier for antifungal and antipruritic peppermint oil emulsion. *Int. J. Biol. Macromol.* **126**, 1014–1022. https://doi.org/10.1016/j.ijbiomac.2018.12.080 (2018).
80. Bibi, A. et al. Recent advances in the production of Exopolysaccharide (EPS) from *Lactobacillus* spp. and its application in the Food Industry: A review. *Sustainability* **13**, 12429. https://doi.org/10.3390/su132212429 (2021).
81. Okaiyeto, K., Nwodo, U. U., Mabinya, L. V. & Okoh, A. I. Characterization of a bioflocculant produced by a consortium of *Halomonas* sp. Okoh and *Micrococcus* Sp.. *Leo Int. J. Environ. Res. Public Health* **10**, 5097–5110. https://doi.org/10.3390/ijerph10105097 (2013).
82. Mathivanan, K. et al. Characterization and biotechnological functional activities of exopolysaccharides produced by *Lysinibacillus fusiformis* KMNTT-10. *J. Polym. Environ.* **29**, 1742–1751. https://doi.org/10.1007/s10924-020-01986-3 (2021).
83. Verstrepen, K. J. & Klis, F. M. Flocculation, adhesion and biofilm formation in yeasts. *Mol. Microbiol.* **60**, 5–15. https://doi.org/10.1111/j.1365-2958.2006.05072.x (2006).
84. Insulkar, P., Kerkar, S. & Lele, S. S. Purification and structural-functional characterization of an exopolysaccharide from Bacillus licheniformis PASS26 with in-vitro antitumor and wound healing activities. *Int. J. Biol. Macromol.* **120**, 1441–1450. https://doi.org/10.1016/j.ijbiomac.2018.09.147 (2018).

85. Kumari, S., Annamareddy, S. H. K., Abanti, S. & Rath, P. K. Physicochemical properties and characterization of chitosan synthesized from fish scales, crab and shrimp shells. *Int. J. Biol. Macromol.* **104**, 1697–1705. https://doi.org/10.1016/j.ijbiomac.2017.04.119 (2017).
86. Trabelsi, I. et al. Physicochemical, technofunctional, and antioxidant properties of a novel bacterial exopolysaccharide in cooked beef sausage. *Int. J. Biol. Macromol.* **111**, 11–18. https://doi.org/10.1016/j.ijbiomac.2017.12.127 (2018).
87. INN-Chile (a). Calidad del Agua—Muestreo—Parte 2: Guía Sobre Técnicas de Muestreo; Norma Chilena Oficial NCh 411/2. Of96 16 (Instituto Nacional de Normalización, 1999).
88. INN-Chile (b). Calidad del Agua—Muestreo—Parte 3: Guía Sobre Preservación y Manejo de las Muestras; Norma Chilena Oficial NCh 411/3. Of96. p 40 (Instituto Nacional de Normalización, 1999).
89. INN-Chile (c). Calidad del Agua—Muestreo—Parte 10: Guía Para el Muestreo de Aguas Residuales; NCh 411/10 Of 97 (Instituto Nacional de Normalización, 1999).
90. Standard Methods for the Examination of Water and Wastewater. APHA, AWWA and WPLF. Ed. 18. a. pp. 2–56, (1992)b pp. 4-100, (1992)c pp. 4–85. (1992).
91. Fierro, P., Tapia, J., Bertrán, C., Acuña, C. & Vargas-Chacoff, L. Assessment of heavy metal contamination in two edible fish species and water from north patagonia estuary. *Appl. Sci.* **11**(6), 2492. https://doi.org/10.3390/app11062492 (2021).
92. Marín-Sanhueza, C. et al. Stress dependent biofilm formation and bioactive melanin pigment production by a thermophilic Bacillus species from Chilean hot spring. *Polymers*. **14**(4), 680. https://doi.org/10.3390/polym14040680 (2022).
93. Frank, J. A. et al. Critical evaluation of two primers commonly used for amplification of bacterial 16S rRNA genes. *Appl. Environ. Microbiol.* **74**(8), 2461–2470. https://doi.org/10.1128/AEM.02272-07 (2008).
94. Tamura, K. & Nei, M. Estimation of the number of nucleotide substitutions in the control region of mitochondrial DNA in humans and chimpanzees. *Mol. Biol. Evol.* **10**(3), 512–526. https://doi.org/10.1093/oxfordjournals.molbev.a040023 (1993).
95. Kumar, S., Stecher, G. & Tamura, K. MEGA7: Molecular evolutionary genetics analysis version 7.0 for bigger datasets. *Mol. Biol. Evol.* **33**(7), 1870–1874. https://doi.org/10.1093/molbev/msw054 (2016).
96. Wick, R. R., Judd, L. M. & Holt, K. E. Performance of neural network basecalling tools for Oxford Nanopore sequencing. *Genome Biol.* **20**, 1–10. https://doi.org/10.1186/s13059-019-1727-y (2019).
97. Kolmogorov, M. et al. metaFlye: Scalable long-read metagenome assembly using repeat graphs. *Nat. Methods* **17**(11), 1103–1110. https://doi.org/10.1038/s41592-020-00971-x (2020).
98. Li, H. Minimap2: Pairwise alignment for nucleotide sequences. *Bioinformatics* **34**, 3094–3100. https://doi.org/10.1093/bioinformatics/bty191 (2018).
99. Parks, D. H., Imelfort, M., Skennerton, C. T., Hugenholtz, P. & Tyson, G. W. CheckM: Assessing the quality of microbial genomes recovered from isolates, single cells, and metagenomes. *Genome Res.* **25**, 1043–1055. https://doi.org/10.1101/gr.186072.114 (2015).
100. Seemann, T. Prokka: Rapid prokaryotic genome annotation. *Bioinformatics* **30**, 2068–2069. https://doi.org/10.1093/bioinformatics/btu153 (2014).
101. Laslett, D. & Canback, B. ARAGORN, a program to detect tRNA genes and tmRNA genes in nucleotide sequences. *Nucleic Acids Res.* **32**, 11–16. https://doi.org/10.1093/nar/gkh152 (2004).
102. Grant, J. R. & Stothard, P. The CGView server: A comparative genomics tool for circular genomes. *Nucleic Acids Res.* **36**, W181–W184. https://doi.org/10.1093/nar/gkn179 (2008).
103. Richter, M., Rosselló-Móra, R., Glöckner, O. & Peplies, J. JspeciesWS: A web server for prokaryotic species circumscription based on pairwise genome comparison. *Bioinformatics* **32**, 929–931. https://doi.org/10.1093/bioinformatics/btv681 (2016).
104. Yoon, S. H. et al. Introducing EzBioCloud: A taxonomically united database of 16S rRNA gene sequences and whole-genome assemblies. *Int. J. Syst. Evol. Microbiol.* **67**, 1613–1617. https://doi.org/10.1099/ijsem.0.001755 (2016).
105. Aziz, R. K. The RAST server: Rapid annotations using subsystems technology. *BMC Genom.* **9**, 1–15. https://doi.org/10.1186/1471-2164-9-75 (2008).
106. Blin, K. et al. antiSMASH 7.0: New and improved predictions for detection, regulation, chemical structures and visualisation. *Nucleic Acids Res.* **51**(W1), W46–W50. https://doi.org/10.1093/nar/gkad344 (2023).
107. Goris, J. DNA–DNA hybridization values and their relationship to whole-genome sequence similarities. *IJSEM.* **57**(1), 81–91 (2007).
108. de Pedrosa, F., Schols, L., de Vos, H., Fabi, J. P. & P., & Assessing high-temperature and pressure extraction of bioactive water-soluble polysaccharides from passion fruit mesocarp. *Carbohydr. Polym.* 122010. https://doi.org/10.1016/j.carbpol.2024.122010 (2024).
109. Donadio, J. L. et al. Ripe papaya pectins inhibit the proliferation of colon cancer spheroids and the formation of chemically induced aberrant crypts in rats colons. *Carbohydr. Polym.* **331**, 121878. https://doi.org/10.1016/j.carbpol.2024.121878 (2024).
110. Da Silva, M. P., Rosales, T. K. O., de Freitas Pedrosa, L. & Fabi, J. P. Creation of a new proof-of-concept pectin/lysozyme nanocomplex as potential β-lactose delivery matrix: Structure and thermal stability analyses. *Food Hydrocoll.* **134**, 108011. https://doi.org/10.1016/j.foodhyd.2022.108011 (2023).
111. do Prado, S. B. R., Santos, G. R., Mourão, P. A. & Fabi, J. P. Chelate-soluble pectin fraction from papaya pulp interacts with galectin-3 and inhibits colon cancer cell proliferation. *Int. J. Biol. Macromol.* **126**, 170–178. https://doi.org/10.1016/j.ijbiomac.2018.12.191 (2019).
112. Nitha, B., De, S., Adhikari, S. K., Devasagayam, T. P. A. & Janardhanan, K. K. Evaluation of free radical scavenging activity of morel mushroom, Morchella esculenta mycelia: A potential source of therapeutically useful antioxidants. *Pharm. Biol.* **48**(4), 453–460. https://doi.org/10.3109/13880200903170789 (2010).
113. Ruch, R. J., Crist, K. A. & Klaunig, J. E. Effects of culture duration on hydrogen peroxide-induced hepatocyte toxicity. *Toxicol. Appl. Pharmacol.* **100**(3), 451–464. https://doi.org/10.1016/0041-008X(89)90293-7 (1989).
114. Benzie, I. F. & Strain, J. J. The ferric reducing ability of plasma (FRAP) as a measure of antioxidant power: The FRAP assay. *Anal. Biochem.* **239**(1), 70–76. https://doi.org/10.1006/abio.1996.0292 (1996).
115. Cooper, D. G. & Goldenberg, B. G. Surface-active agents from two Bacillus species. *Appl. Environ. Microbiol.* **53**(2), 224–229. https://doi.org/10.1128/aem.53.2.224-229.1987 (1987).
116. Kanmani, P., Yuvaraj, N., Paari, K. A., Pattukumar, V. & Arul, V. Production and purification of a novel exopolysaccharide from lactic acid bacterium Streptococcus phocae PI80 and its functional characteristics activity in vitro. *Bioresour. Technol.* **102**(7), 4827–4833. https://doi.org/10.1016/j.biortech.2010.12.118 (2011).
117. Pu, L. et al. Using a novel polysaccharide BM2 produced by Bacillus megaterium strain PL8 as an efficient bioflocculant for wastewater treatment. *Int. J. Biol. Macromol.* **162**, 374–384. https://doi.org/10.1016/j.ijbiomac.2020.06.167 (2020).
118. Wang, J. C. & Kinsella, J. E. Functional properties of novel proteins: Alfalfa leaf protein. *J. Food Sci.* **41**, 286–292. https://doi.org/10.1111/j.1365-2621.1976.tb00602 (1676).

Acknowledgements

A.B., G.C-B., and J.P.F. acknowledge Fondecyt Regular 1231917 by ANID, Govt. of Chile. A.B., G.C-B., S.S., J.P.F., and R.K.S. also acknowledge FOVI 220149 by ANID, Govt. of Chile. G.C-B acknowledge Fondecyt Regular 1221609. The National Council for Scientific and Technological Development (CNPq) for J.P.F. productivity scholarship (#307842/2022-3). The São Paulo Research Foundation (FAPESP) for #2013/07914-8.

Author contributions

Conceptualization and Methodology, A.B.; Experiments, S.S., G.C-B., R.N.S, J.P.F., S.J.M.B, J.T, A.B, Manuscript preparation, S.S., G.C-B., R.N.S, J.P.F, S.J.M.B, J.T and A.B., Revision and Editing, S.S., G.C-B., R.N.S, J.P.F, J.T, R.K.S and A.B., Resource, R.K.S., J.P.F, and A.B. Funding acquisition, A.B. All authors have agreed to the published version of the manuscript.

Funding

This research was funded by FONDECYT Regular, Grant Number 1231917, by ANID, Govt. of Chile.

Declarations

Competing interests

The authors declare no competing interests.

Additional information

Supplementary Information The online version contains supplementary material available at https://doi.org/10.1038/s41598-024-74830-6.

Correspondence and requests for materials should be addressed to A.B.

Reprints and permissions information is available at www.nature.com/reprints.

Publisher's note Springer Nature remains neutral with regard to jurisdictional claims in published maps and institutional affiliations.